# 6. STRUCTURE

FIGURE 6.1 (OVERLEAF).—Lee-Lincoln scarp west of Apollo 17 landing site, partly covered by light-colored landslide of debris from South Massif (bottom). Scene centered at 20.25° N., 30.75° E., covers 7.5 km north-south. Apollo 17 frame P–2309.

# 6. STRUCTURE

CONTENTS



## INTRODUCTION

Tectonic structures, like endogenic materials, play a smaller role in lunar geology than was once widely thought. Miscellaneous aligned landforms were interpreted as fault-controlled during much of the telescopically based mapping of the 1960's. Geologists commonly mapped faults without the objectivity that proved so valuable in mapping material units. Basin rings were generally mapped as fault-bounded, and lineament trends were commonly assigned to the "lunar grid," a hypothetical system of conjugate fractures (Fielder, 1961, 1965; Strom, 1964; Mutch, 1970, p. 247–250; Casella, 1976). High-resolution photographs, however, have substantiated the view of some astute early observers that faults are rare on the Moon (Arthur, 1962, p. 321; Baldwin, 1963, chap. 22). Except for the faults described in this chapter and for relatively minor gravitational faulting along some rings, I believe that most supposed faults are coincidental alignments of unrelated features. The lunar grid is probably an artifact of the plotting methods (Wise, 1982).

The present lunar surface, therefore, has not been extensively reshaped by endogenic forces, as has the Earth, but generally retains the pattern imposed by cratering and deposition of stratigraphic units. The dominance of lunar geology by basins and maria extends to most of the tectonic structures that do exist. Most of these structures are inside basins, and many transect both the basin and the mare (pl. 5). Some structures at mare margins that are related to dark pyroclastic materials and irregular craters have already been illustrated (figs. 5.10, 5.16). This chapter more thoroughly describes and interprets basin-related *mare ridges*, *arcuate rilles*, and *crater-floor fractures*.

Some *straight rilles* of fault origin also cut surfaces outside the most conspicuous mare-filled basins. These rilles have not yet been satisfactorily explained. Global deformation is commonly invoked, but this chapter presents alternative, basin-related interpretations for these structures as well. In particular, the 3,200-km-diameter Procellarum basin (Whitaker, 1981), whose importance to terra topography, lithospheric thickness, and mare localization has already been mentioned (chaps. 4, 5; pls. 3, 4; fig. 5.26), is suggested as a major control on the straight rilles as well as the ridges and arcuate faults.

## STRUCTURES IN MARIA AND BASINS

### Mare ridges

Deformation inside mare-filled basins is most manifest in two classes of structures—mare ridges and arcuate grabens. Mare ridges, also known as *wrinkle ridges* and now formally named *dorsa*, are linear positive features that occur in most maria (pl. 5). Most mare ridges are on the nearside because most maria are there, but even small isolated farside maria have ridges (fig. 5.2). Also, some ridges extend from mare margins into the terrae, for example, the "Lee-Lincoln" scarp at the Apollo 17 landing site (fig. 6.1) and some basin-radial ridges south of Mare Humorum (fig. 9.24*B*; Saunders and Wilhelms, 1974). The ridges generally occur in systems that are subconcentric and subradial to maria (pl. 5; figs. 5.17, 5.23*A*, 6.2). Systems in Oceanus Procellarum (fig. 6.3), which appear to be linear and parallel (Scott, 1974), are concentric with the Procellarum basin (fig. 5.26*B*; Whitaker, 1981).

In detail, mare ridges consist of linear segments that merge, overlap, or are arranged in echelon (figs. 6.2, 6.3); many extend as complex, branching echelon systems for hundreds of kilometers. Ridges generally have two distinct morphologic parts—a broad arch and a narrow superposed spine (Strom, 1971). Some arches are composed of overlapping domes. They range from several kilometers to as much as 10 km in width and commonly are about 100 m high; in Mare Serenitatis, some arches reach a height of 350 m (fig. 6.2; Muehlberger, 1974). Such large arches appear on all photographs, but many others appear only on photographs taken at low-Sun illuminations (less than 15°) and are not necessarily disclosed by high photographic resolutions. Many arches are asymmetric, bounded on one side by scarps or monoclinal bends that offset the mare surface by 50 to 100 m (Lucchitta, 1976). In places, the asymmetry shifts sides along the length of the ridge. Some scarps resemble flow lobes in shape. The sharp spinelike ridges commonly form shorter, narrower, tortuously braided networks along the crests and flanks of the broader arches, and may occupy 25 to 60 percent of the total arch width (figs. 6.2, 6.3; Strom, 1971). The spines are commonly 100 m high and about 200 m wide (Lucchitta, 1976). Some spines extend from the arches onto the

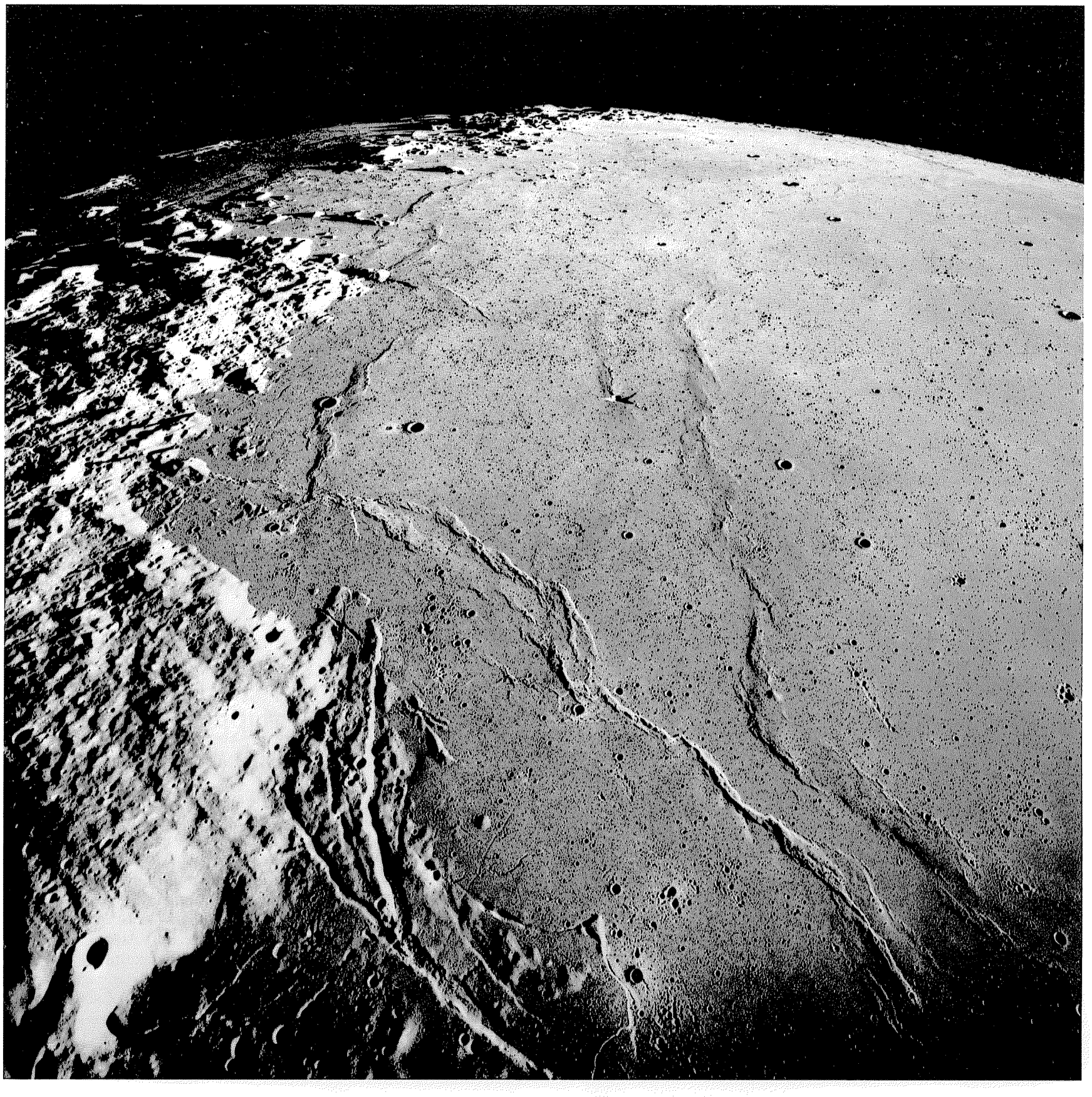

FIGURE 6.2.—Border zone between Mare Serenitatis and Serenitatis-basin rim, showing structures concentric with mare. View northward.

*A*. West and southwest border. Rugged terra is Montes Apenninus. Grabens concentric with and truncated by mare are Rimae Sulpicius Gallus (compare fig. 5.16). Apollo 17 frame M–952.

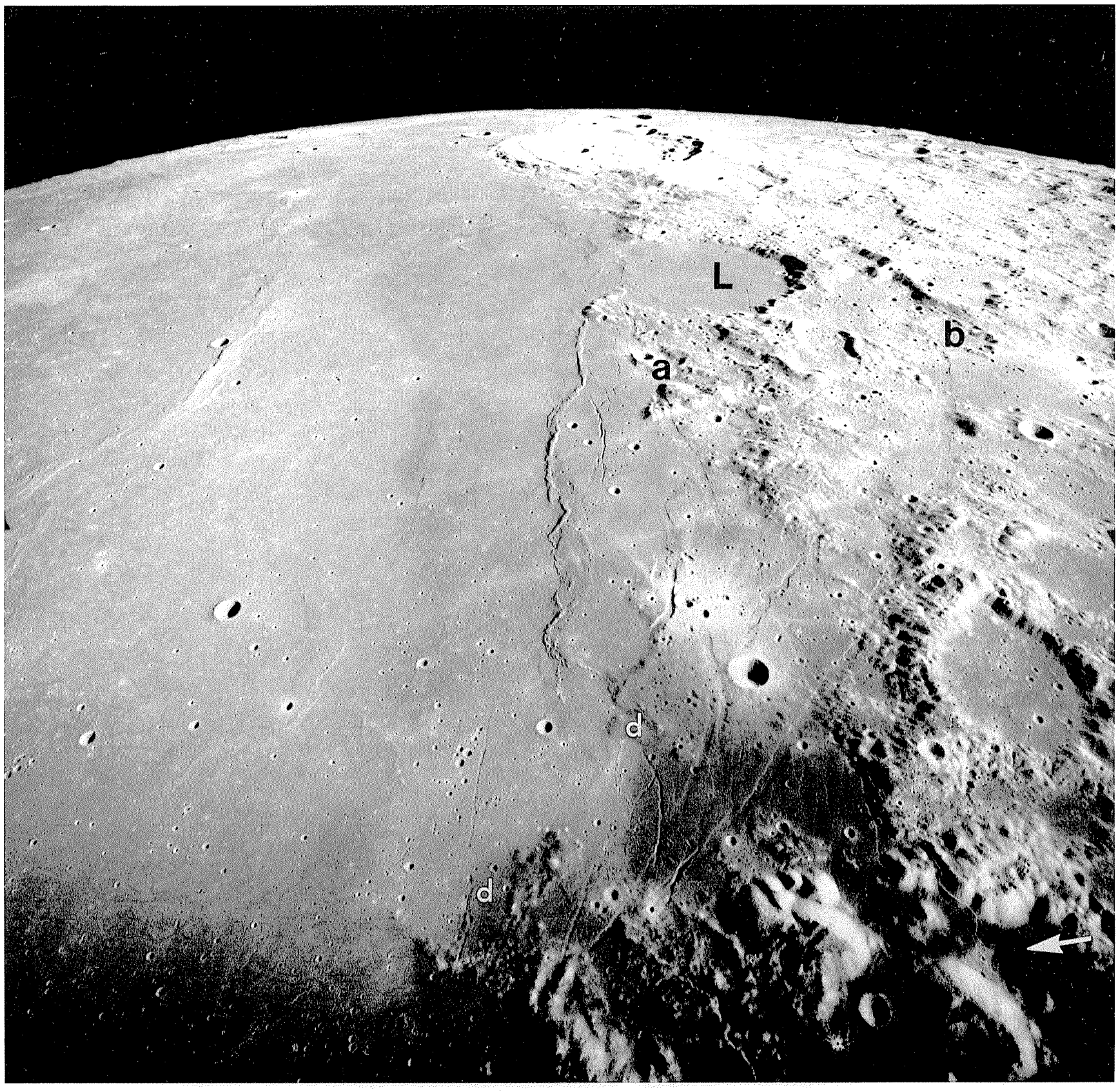


*B*. East border. Two sets of grabens diverge upward from near bottom of photograph; one is closely concentric with the mare (a), and the other diverges eastward (b). L, LeMonnier (61 km, 27° N., 31° E.). Dark-mantling material at bottom (d) is truncated by lighter central mare. Arrow, Apollo 17 landing site (compare fig. 5.17). Apollo 17 frame M–940.

adjacent flat mare surfaces; others are solitary. In some places, both the arches and the narrow spines are superposed on gentle linear rises, as much as 500 m high and 25 km wide, that can be detected only on low-Sun images or by topographic data (Lucchitta, 1976).

Two main schools of interpretation of mare ridges have emerged. The volcanic school favors intrusion and extrusion of lava, controlled by global or basin-related tectonic patterns (Fielder, 1965; Quaide, 1965; Hartmann and Wood, 1971; Strom, 1971; Scott, 1974), or a variant—autointrusion of lavas into fractures (Hodges, 1973c). The tectonic school, which was founded by Baldwin (1963, p. 380–382; 1968), favors structural deformation of solid materials and is supported by the studies discussed in this chapter. Most investigators agree that many circular wrinkle ridges were formed by compaction over crater rims (fig. 6.4). Other, larger circular patterns of mare ridges are ascribed to settling of mare sections over buried basin rings; such ridges are, in fact, the only basis for locating the inner rings of Imbrium, Serenitatis, Crisium, and other deeply filled basins (table 4.1; Hartmann and Kuiper, 1962; Hartmann and Wood, 1971; Wilhelms and McCauley, 1971; Maxwell and others, 1975; Brennan, 1976).

Many exposed parts of crater rims, basin rings, and other buried terrae assume domelike landforms (figs. 6.5*A*, *B*). These landforms and the associated ridges have been interpreted as ringlike volcanic complexes. The moldinglike accumulations of material at the bases of the terra remnants resemble volcanic flows (O'Keefe and others, 1967; Strom, 1971), and their light color implies silicic composition. However, the "moldings" are common along contacts between mare surfaces and terra slopes, including those of obvious impact features (figs. 6.1, 6.5), where they consist of debris accumulated from the slopes (Milton, 1967; Offield, 1972). Therefore, these accumulations are stratigraphically younger than the ridges and the mare materials at the bases of the terra islands, whereas their source bedrock is older than the maria.

Evidence for dislocations of nonmare units (figs. 6.6, 6.7) has led to elaboration of the tectonic hypothesis. The complex ridge morphology suggests crumpling of the surface under compressional stress. Howard and Muehlberger (1973) suggested that the compression created thrust faults along intramare gliding horizons. Bryan (1973) and Maxwell and others (1975) explained the compression as a

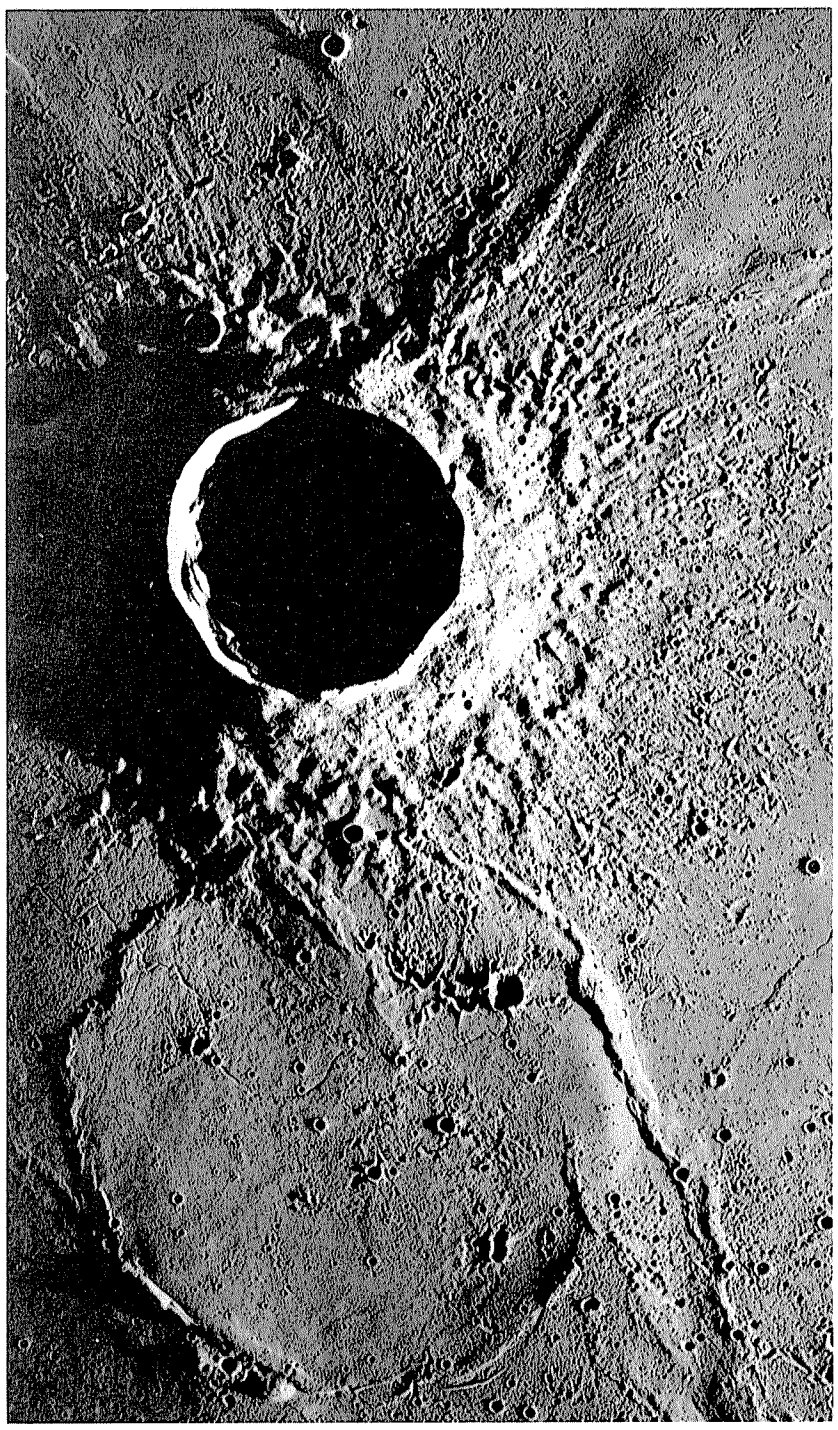

FIGURE 6.4.—Mare ridges, formed by subsidence of mare basalt over rim of crater Lambert R (bottom; 55 km, 24° N., 20.5° W.). Unburied crater with shadowed interior above center is Lambert (30 km). Apollo 15 frame M–1010.

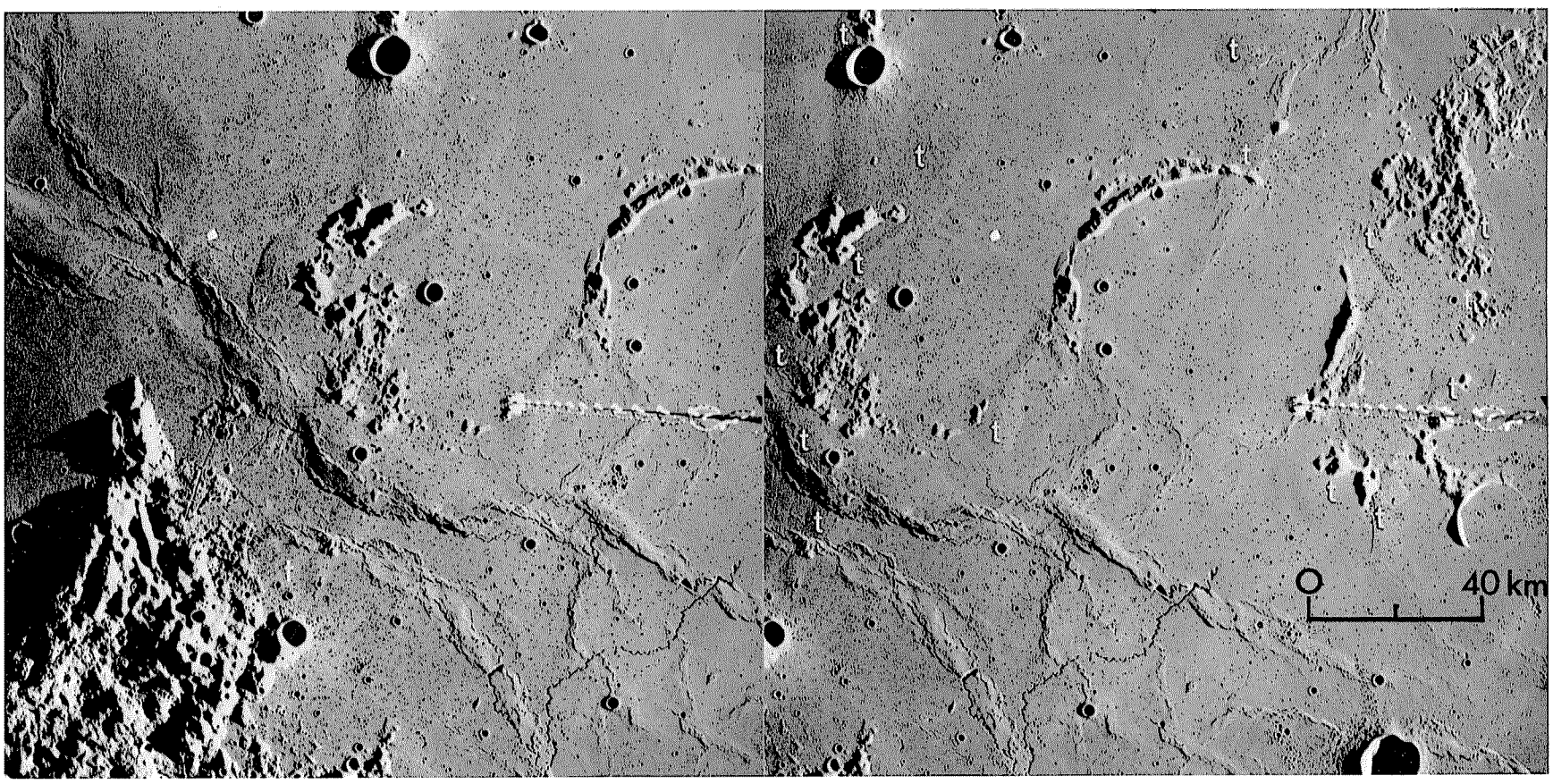


FIGURE 6.3.—Complex mare ridges and flooded terra islands in southern Oceanus Procellarum near crater Letronne (left edge of left frame; Colton and others, 1972). Some ridges and kipukas or steptoes of elevated, presumably thin maria (t) mark subsurface extensions of crater rims and other terra. Photograph covers area of lat 7.0°–13.5° S., long 32.5°–41.5° W. Object at center right of both frames is boom of Apollo 16 gamma-ray spectrometer. Stereoscopic pair of Apollo 16 frames M–2837 (right) and M–2839 (left).

buckling of the surface caused by settling of the maria into a reduced area; thick sections of mare basalt settle most, and the stresses are concentrated where the basalt thins (Maxwell and others, 1975). Lucchitta (1976, 1977b) also favored settling and suggested that the ridges lie along fault systems that include both normal and reverse faults, which are manifested by compression at the surface (fig. 6.8). In these hypotheses, accepted here, most ridges originate basically by compression resulting from vertical tectonism, although some are probably of volcanic origin (fig. 5.13).

## Arcuate rilles

Arcuate rilles (*rimae*) are flat-floored, steep-walled troughs (figs. 6.9, 6.10, 6.11). Each trough consists of a floor a few kilometers wide and linear subparallel facing scarps 50 to 250 m high (Golombek, 1979). The troughs are grabens created by extension, like many similar grabens on the Earth (Baldwin, 1949, p. 197–199; 1963; Quaide, 1965; McGill, 1971; Golombek, 1979). Like the ridges, most arcuate grabens occur in parallel, crosscutting, or echelon sets; some occur

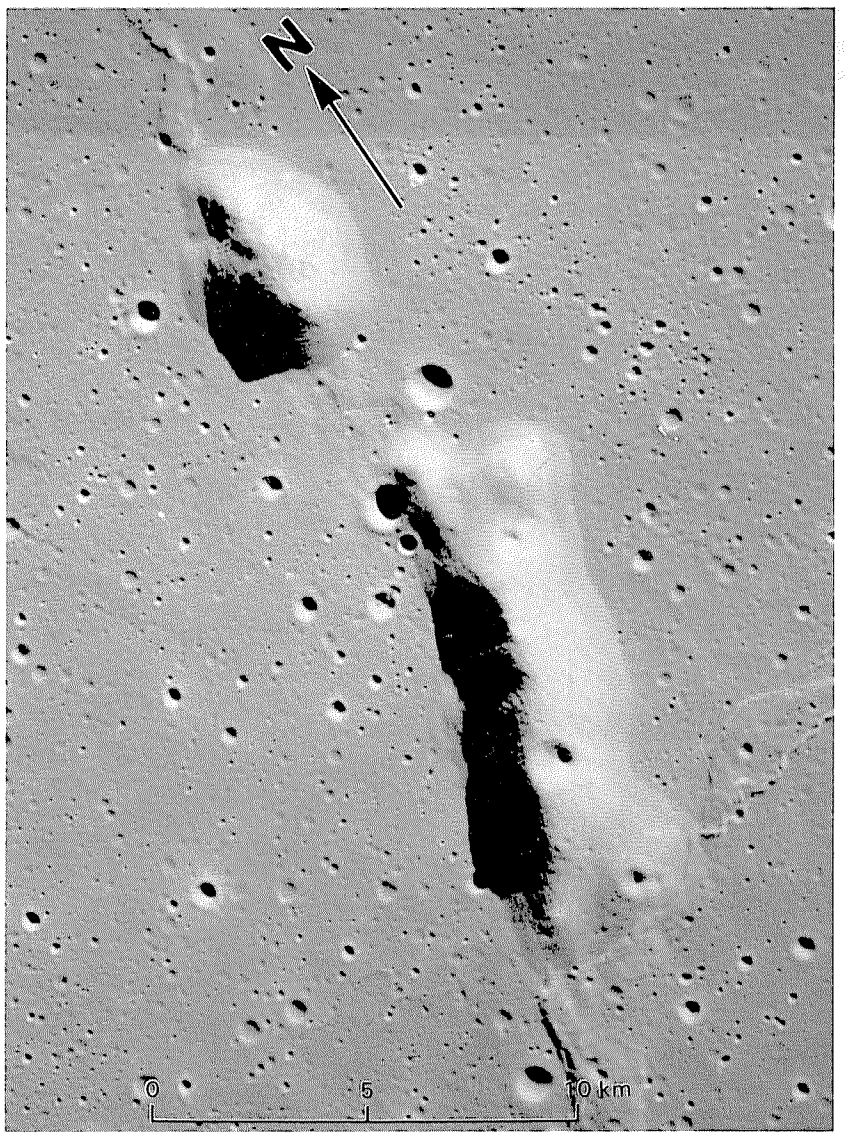


A

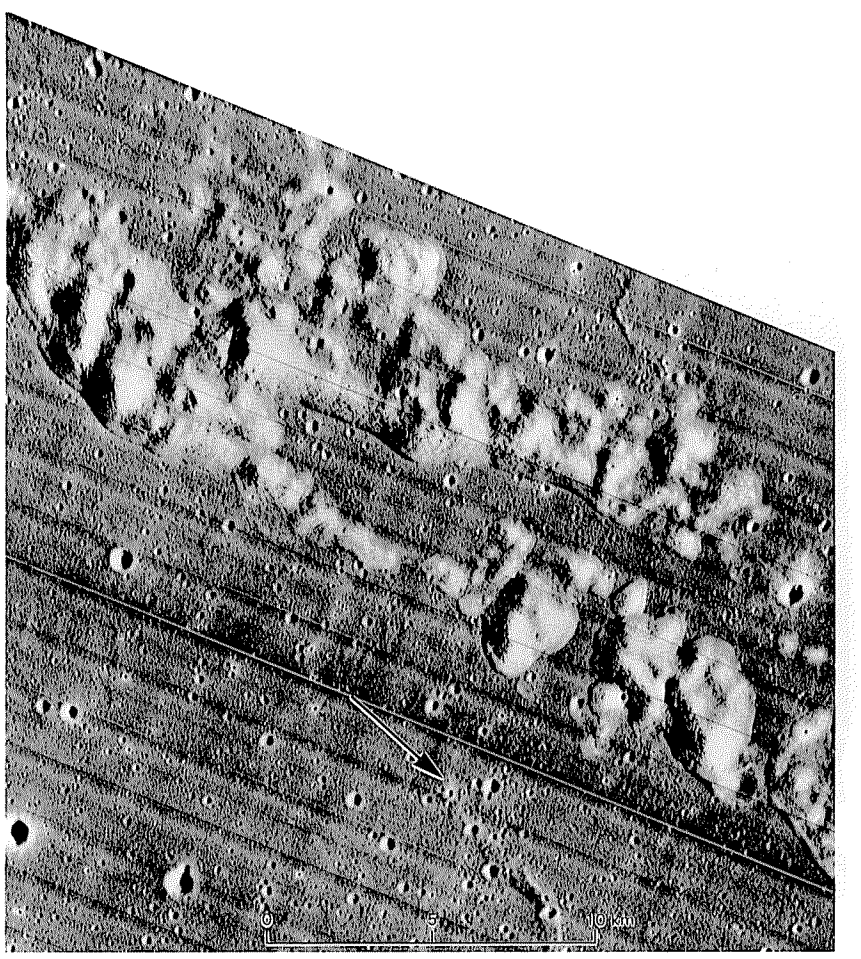


B

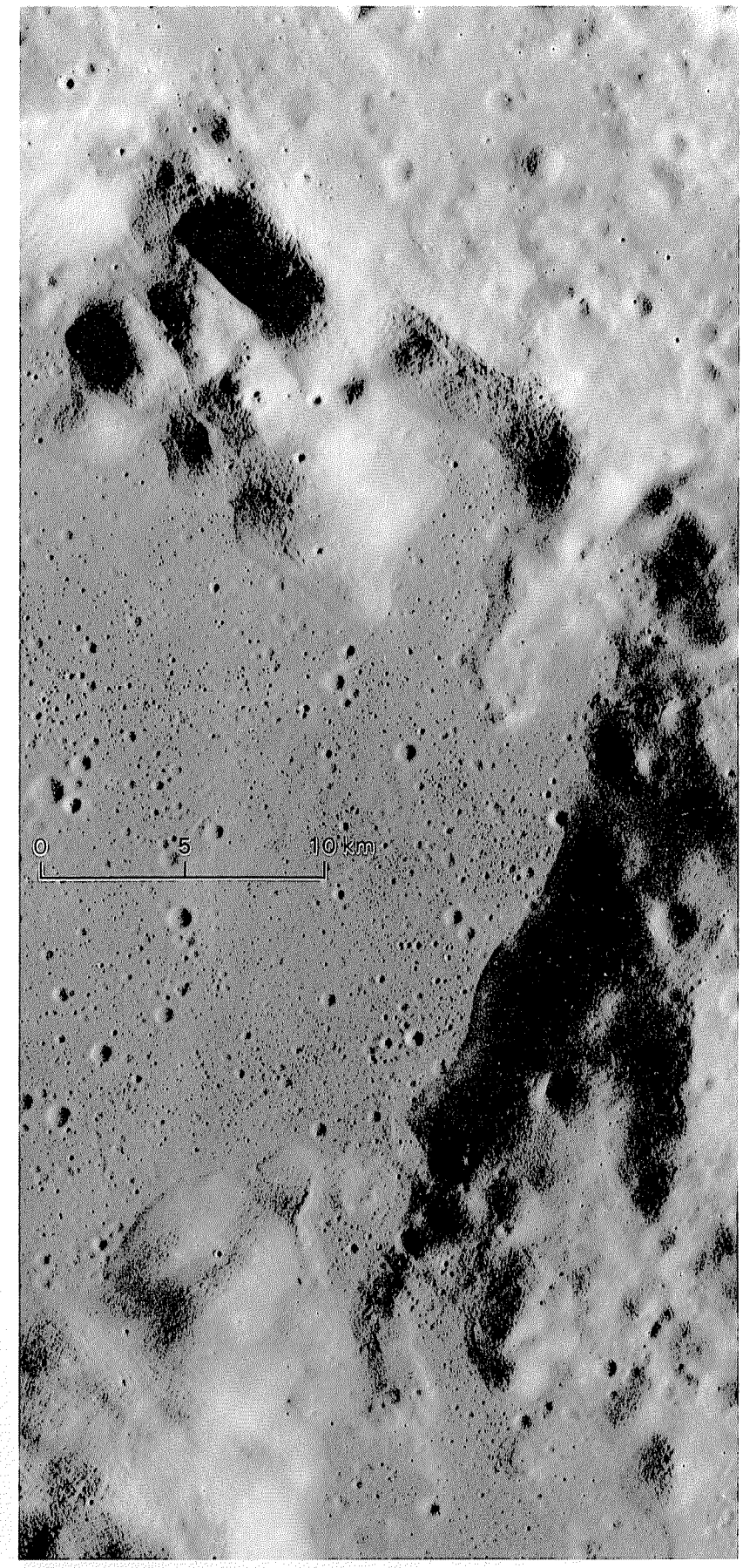


C

FIGURE 6.5.—Moldinglike accumulations of debris at bases of partly inundated impact features.

*A*. Light-colored domelike features along mare ridge are terra islands that partly deflect the ridges. Apollo 16 frame H–19244.

*B*. Part of crater Flamsteed P ("Flamsteed Ring") concentric with mare ridge (arrow). Orbiter 3 frame M–181.

*C*. Interior of crater Maraldi. Apollo 17 frame P–2302.

singly. Most grabens are concentric with circular maria and the containing basins (pl. 5; figs. 5.16, 5.17, 6.9–6.11). Moreover, they lie within the topographic-basin rim as that rim is interpreted in chapter 4 (except for some subconcentric grabens east of Serenitatis, which may be controlled by the middle Procellarum-basin rim; set b, fig. 6.2*B*). Grabens cut both the mare and the basin material (figs. 6.9, 6.10). With minor exceptions, they occur only in basins superposed on the Procellarum basin, particularly Imbrium, Serenitatis, Tranquillitatis, and Humorum (pl. 5), and are rare or absent in the large basins Crisium, Nectaris, and Smythii and on the farside.

## *Origin by mare subsidence*

The recurring association of mare ridges and arcuate grabens suggests a genetic connection (Baldwin, 1963, 1968). Their geometric relation is similar in many basins: Subradial ridges innermost, arcuate rilles outermost, and concentric ridges in between. Discovery of the mascons (chap. 5; Muller and Sjogren, 1968) led to the currently prevailing interpretation, which substantiates Baldwin's (1963, p. 380–382) concept. The mare-basalt masses constitute the superisostatic loads in the mascon basins (Baldwin, 1968; Wise and Yates, 1970; Phillips and others, 1972; Bowin and others, 1975; Sjogren and Smith, 1976; Melosh, 1978; Solomon and Head, 1979, 1980). These superisostatic loads are generally smaller than they would be if no isostatic compensation had taken place since mare emplacement began (Solomon and Head, 1980, p. 136); therefore, the basalt must have subsided. This subsidence stretched the peripheral parts of the mare and the basin floor, creating the grabens, and compressed the center, creating the ridges (fig. 6.12; Baldwin, 1968; Melosh, 1978; Solomon and Head, 1979, 1980).

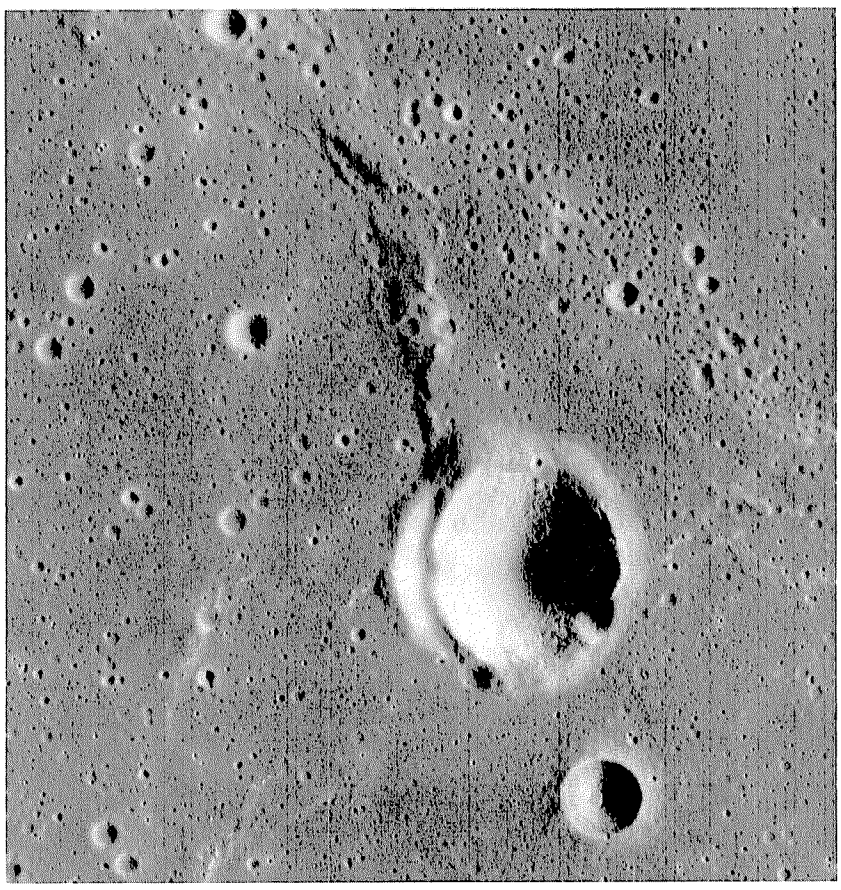

FIGURE 6.6.—Crater Bonpland D (6 km, 10° S., 18° W.) in Mare Cognitum, offset along mare ridge. Apollo 16 frame P–5429.

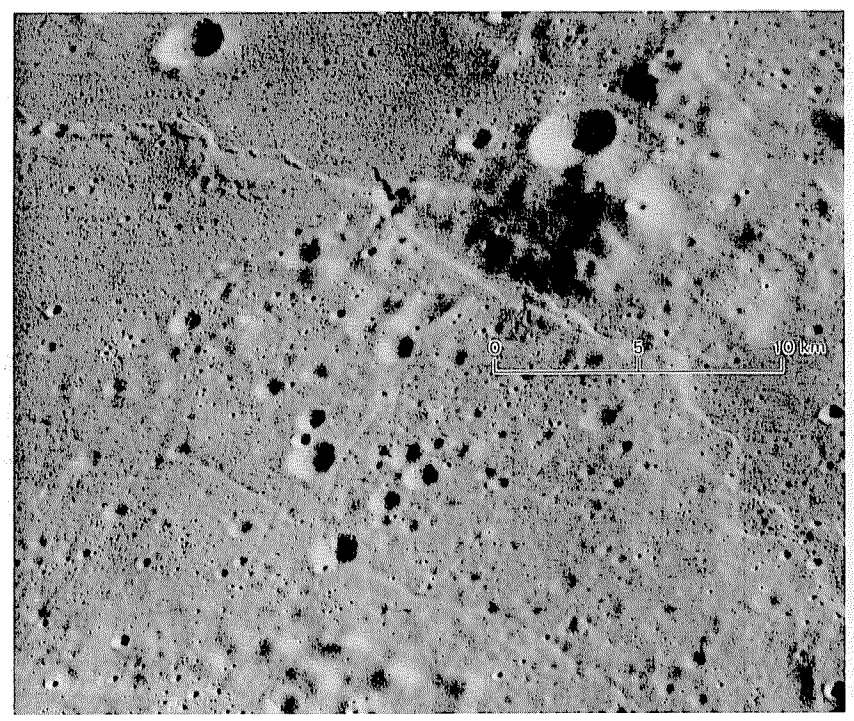


FIGURE 6.7.—Ridges continuous between mare and terra and appearing to thrust material from bottom over material at top. Scene centered at 7° S., 29° W., in Montes Riphaeus. View northward. Apollo 16 frame P–5452.

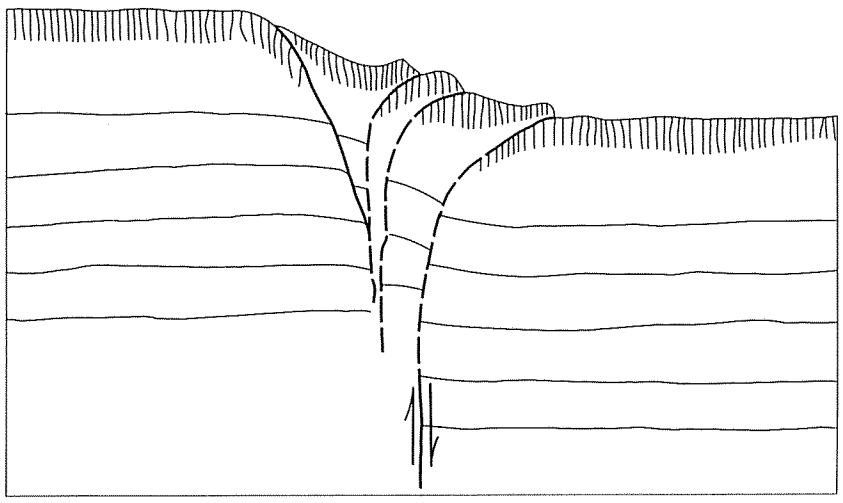

FIGURE 6.8.—Interpretation of mare ridges by Lucchitta (1976), based on models by A.R. Sanford. Thrust relations on surface originate by vertical displacements along steep faults in subsurface. Normal faulting occurs under tension in relatively raised block.

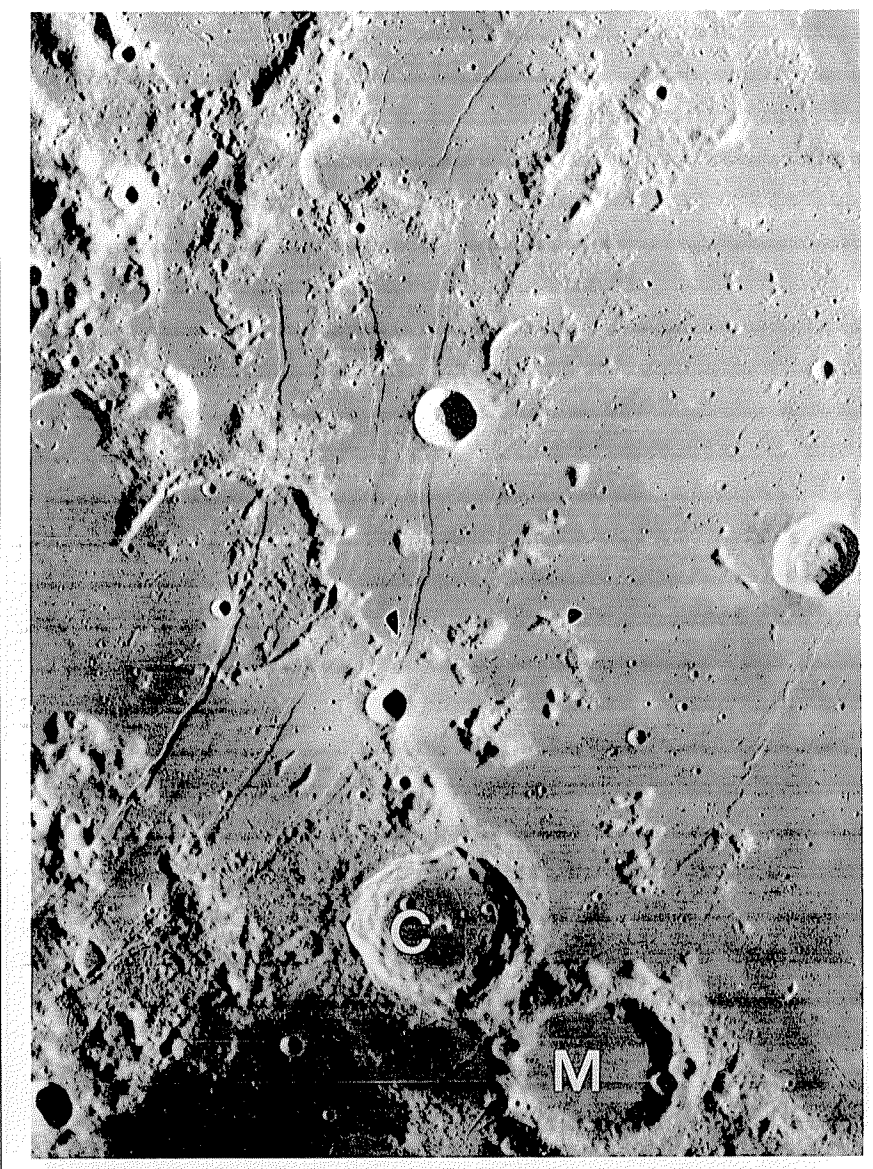


FIGURE 6.9.—Arcuate rilles concentric with Mare Humorum and Humorum basin, between southeastern Mare Humorum (left) and westward extension of Mare Nubium (right). Craters include Campanus (C; 48 km, 28° S., 29° W.) and more highly degraded Mercator (M; 47 km). Orbiter 4 frame H–132.

# CRATER-FLOOR FRACTURES

Fractures in the floor materials of craters are among the commonest lunar tectonic structures (figs. 6.13, 6.14). They are concentrated in and near maria and basins without maria (pl. 5). Fractured-floor craters larger than about 150 km also occur in nonbasin settings, for example, Petavius and Humboldt (figs. 4.2, 9.5, 9.6). These two craters are gravitationally neutral; they have neither the negative anomalies of fresh craters nor the positive anomalies due to mare basalt (Dvorak and Phillips, 1978).

The fractured floors are higher relative to the crater rims and surrounding terrain than are the floors of typical impact craters (Pike, 1971). Many of the floors, however, occur in craters with other morphologies diagnostic of impact origin—such as central peaks, as in Gassendi and Posidonius (figs. 5.17, 6.13*A*), and the whole range of exterior impact phenomena including rays, as at Taruntius (fig. 6.13*B*). Uplift of impact-crater floors is the evident explanation. The presence of fractured floors in Petavius and Humboldt (fig. 4.2) suggests that originally negative gravity anomalies resulting from mass loss during impact excavation were erased by the uplifts. Vitello on the Mare Humorum border (fig. 6.13*C*) possesses a freshly fractured floor, a mantle of dark material, and an enhancement in thermal-infrared wavelengths during eclipse (Shorthill and Saari, 1969)—all features pointing to a caldera origin or, at least, to eruptions from the floor fractures (Saunders and Wilhelms, 1974). However, these features are also consistent with floor uplift (fig. 6.15), which opened fissures fresh enough to expose blocks that appear "warm" during eclipse, and with mantling by the dark material—a common phenomenon along other mare borders as well (Titley, 1967).

The uplift interpretation also suggests an explanation for a wide range of other lunar landforms (Brennan, 1975; Schultz, 1976a). The shallow tilted floors and arcuate structures of 15 craters larger than 20 km in diameter in the Smythii basin (fig. 6.13*E*; Wilhelms and El-Baz, 1977) suggest cylinderlike uplifts that broke free where the wall and floor meet (fig. 6.15). Especially great uplift probably formed the irregular, knobby elevated interior of Gaudibert, along the Mare Nectaris margin (fig. 6.13*F*; Brennan, 1975), which had been thought to be volcanic (Elston, 1972). Even small craters with such elevated interior structures as nested rims or rings of bulbous material (figs. 6.13*D*, *G*) may be modified by tectonic uplift rather than by volcanism, as is commonly believed (for example, Schultz, 1976b, p. 12–15). Twin impacts followed by uplift account for the nearly identical neighboring shallow-floored craters Sabine and Ritter along the Tranquillitatis border (fig. 3.14*C*), which superficially resemble terrestrial calderas more than they do impact craters (Morris and Wilhelms, 1967; De Hon, 1971).

Although many fractures and unusual landforms have been created by uplifts of impact-crater floors, a few fractured-floor craters have a less well organized fracture pattern that suggests shrinkage of a cohesive material (fig. 6.13*H*). Most such craters lie near but outside basins, and the fractured material may be impact melt ejected from the basins (Moore and others, 1974; Wilhelms and others, 1979), unless it is otherwise-unknown terra volcanic material (Schultz, 1976b, p. 68; Stuart-Alexander, 1978).

Igneous intrusions have been suggested as the cause of floor uplifts because the uplifts are concentrated near maria and are commonly overlain by dark mantles or small maria (Brennan, 1975; Schultz, 1976a). Intrusions seem reasonable, considering the affected craters' setting. All that is required, however, is isostatic leveling resulting from viscous relaxation of the substrate (Danes, 1965; Hall and others, 1981). The required plasticity is probably due to the weaker lithosphere beneath basins and large craters.

# STRAIGHT RILLES

## General features

More puzzling than the arcuate grabens and floor fractures are rilles that are here called straight by contrast with the other, curved or complexly shaped fractures. Although long stretches are straight (pl. 5; figs. 6.16–6.21), most straight rilles curve or sharply inflect as a whole. In detailed shape of profile and in their echelon patterns, straight and arcuate rilles are similar (fig. 6.16). The straight rilles are also grabens (Quaide, 1965). Some rare single fault scarps not part of a rille are also considered here.

## Imbrium sculpture

Faulting initiated by the Imbrium impact was the preferred explanation during the 1960's for the "Imbrium sculpture" system of radial grooves and ridges (Kuiper, 1959; Shoemaker and Hackman, 1962; Hartmann, 1963, 1964b; Strom, 1964; Wilhelms, 1970b, p. 15; Wilhelms and McCauley, 1971). A coalescence of elliptical craters to form the grooves is evident on Apollo photographs (fig. 3.10*B*), however, confirming the secondary-ejecta origin proposed by Gilbert (1893) and Baldwin (1949, 1963). Nevertheless, some true faults are radial or subradial to Imbrium; those cutting the Apennine Bench, for example, probably formed in response to adjustments of Mare Imbrium and the Imbrium basin (fig. 6.10).

Vallis Alpes (the Alpine Valley, fig. 6.17) lacks the smoothly scalloped matching walls and raised lips characteristic of low-angle secondary chains. Some of its walls match but are jagged, steep, and

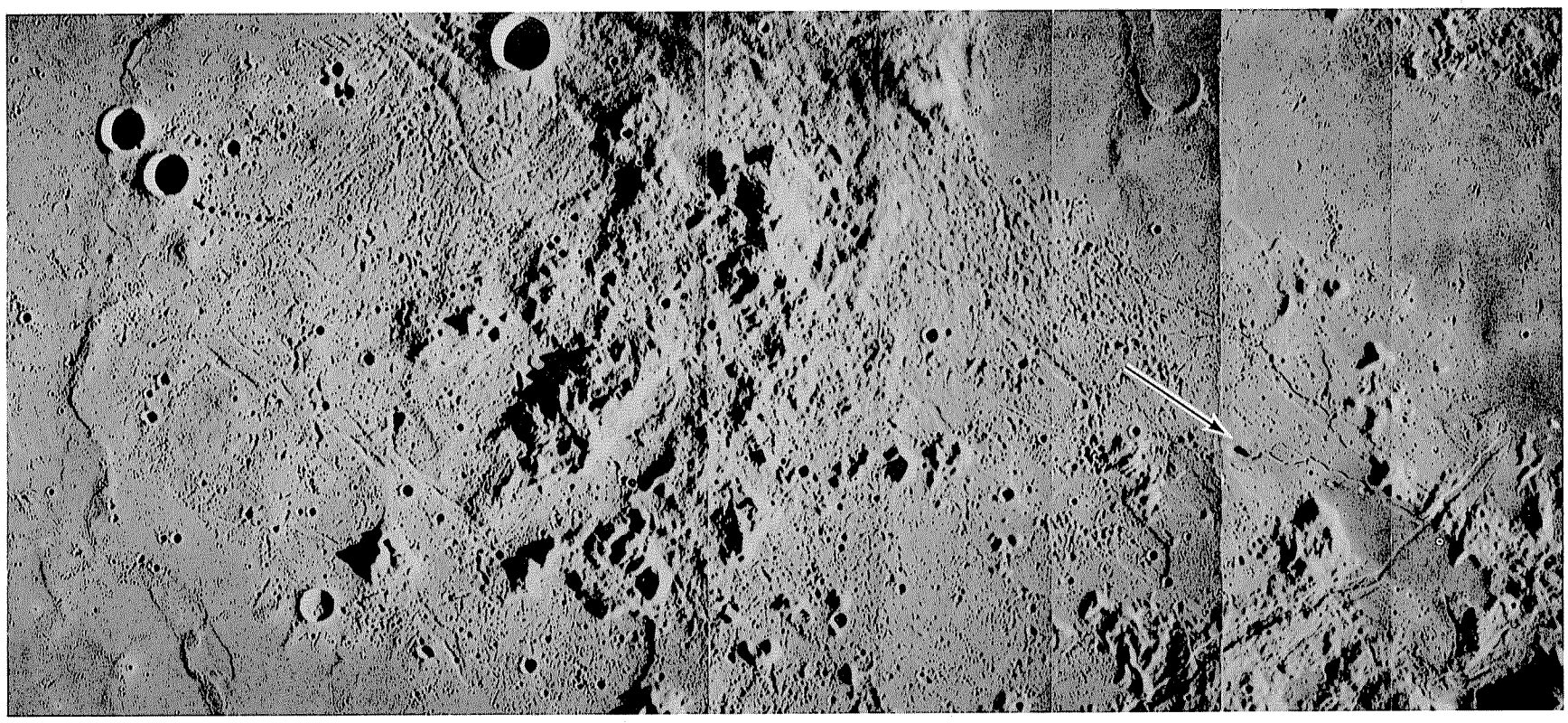

FIGURE 6.10.—Apennine Bench, showing grabens concentric with Imbrium basin cutting basin, bench, and mare material (lower right). Radial grabens and vent for dark-mantling material (arrow) are also present (Imbrium center is outside upper left corner of photograph). Large rugged mass is Montes Archimedes, overlain and surrounded by planar Apennine Bench Formation (see chap. 10) and by secondary craters of Archimedes, centered north of view. Mare at upper right is Palus Putredinis, west of Apollo 15 landing site. Pair of craters at left edge of bench are Feuilleé (left; 9 km) and Beer (9.5 km). Mosaic of Apollo 15 frames M–589 through M–594 (from right to left).

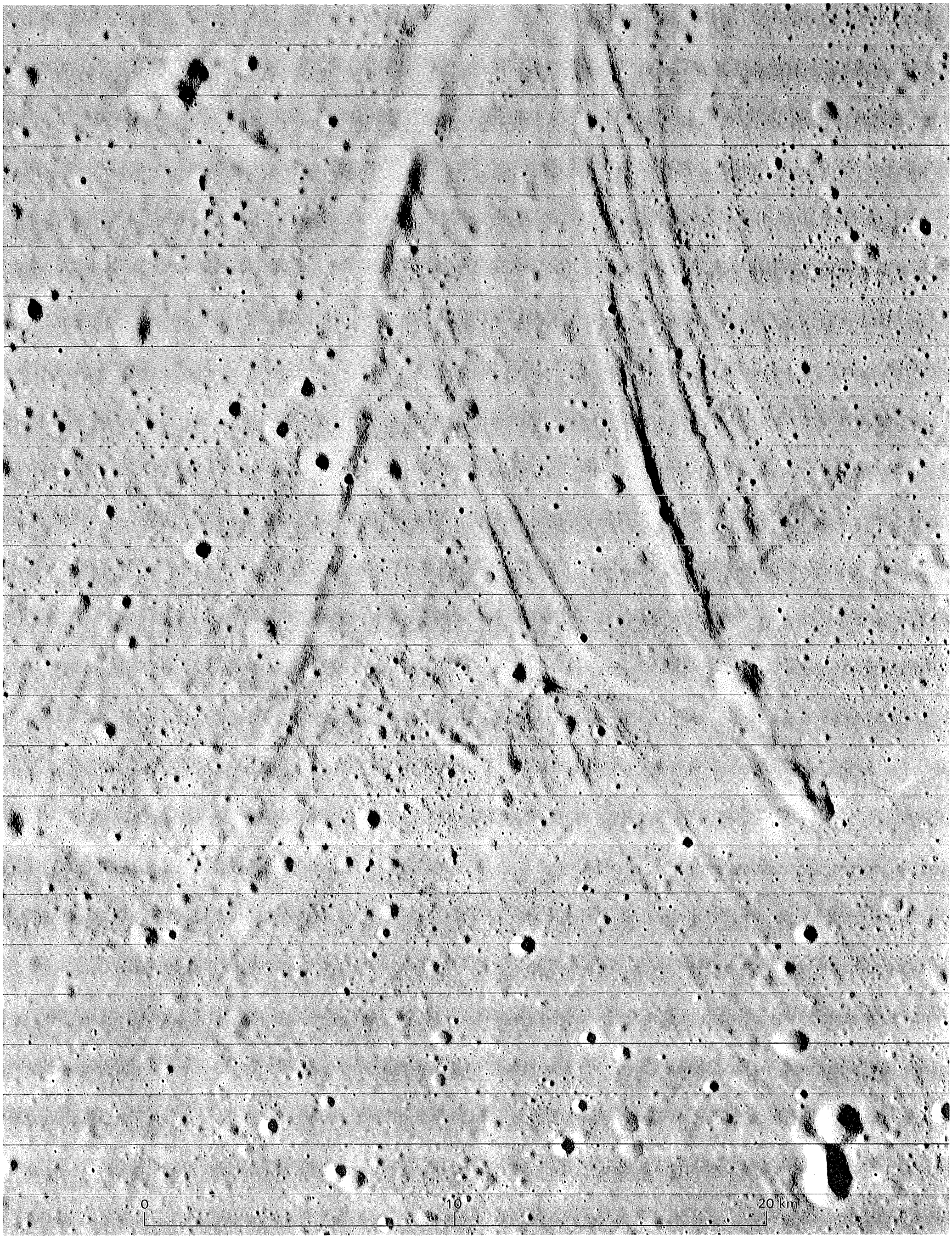


FIGURE 6.11.—Arcuate rilles in border zone of Mare Tranquillitatis (5° N., 21° E.) south of crater Arago, about 90 km east of mare edge. Intricate structure shown here is probably also common in other, less well photographed rille systems. Orbiter 2 frame M–43.

composed of linear segments. The valley is probably a graben formed shortly after the Imbrium impact, as was once proposed for all sculpture. Its radiality is consistent with an origin by isostatic doming of the subbasin mantle (see chap. 4).

Such radial or subradial faults as the Straight Wall (Rupes Recta, fig. 1.8), one leg of Rima Hyginus (figs. 5.10*E*, 6.16*A*), the Cauchy set (fig. 6.18), and several parallel grabens in southwestern Mare Fecunditatis (fig. 6.19) are more puzzling because they cut mare materials. They cannot be direct products of the Imbrium impact. If they are related to Imbrium, they may have formed by some sort of rejuvenation of radial fractures (Wilhelms, 1972a; Holt, 1974; Mason and others, 1976).

## Other systems

The geometric relation of other straight rilles to basins is less apparent. Many grabens in the central and east-central equatorial zone of the nearside are concentrated along trends between 20° and 30° north of west (pl. 5). Most of these grabens belong to a set that extends 1,600 km east-southeastward from Rima Bode II (fig. 5.10*H*), through the eastern leg of Rima Hyginus and Rimae Ariadaeus (fig. 6.16), to the Imbrium-radial rilles in Mare Fecunditatis (figs. 6.19, 9.7). The only basin to which all these grabens are geometrically related is Procellarum, to whose center (23° N., 15° W.; Whitaker, 1981) they are radial or subradial. Their trend is paralleled in other areas by the Cauchy set of structures (also subradial to Procellarum; fig. 6.18), the short Müller crater chain (fig. 3.16*A*), and the 300-km-long Abulfeda crater chain (fig. 3.16*B*). The origin of these crater chains, which are radial to no known basin or large crater, is unclear (see chap. 3). Some grabens near Sinus Medii have a complementary trend of 20°–30° north of east (pl. 5; fig. 10.28).

At the east end of Sinus Medii is the complex Triesnecker system of grabens (pl. 5; fig. 6.20). This system as a whole is oriented north-south but includes many other trends, which mutual transection relations show to be contemporaneous (Wilhelms, 1968). East-west extension is the apparent cause.

The Moon's most complex system of (exposed) grabens occupies the southwest shore of Oceanus Procellarum from about lat 5° N. to lat 22° S. (fig. 6.21). The prevailing trends are nearly concentric with the Procellarum shoreline or radial to the general region of both the Imbrium- and Procellarum-basin centers. Other straight rilles lie along the northwest Procellarum shore, which also contains the largest lunar concentration of fractured-floor craters (pl. 5; fig. 6.14).

# INTERPRETATION—LITHOSPHERIC THICKNESS

Many, if not most, of the structures described in this chapter are ascribable to thinning of the elastic lithosphere beneath basins. The subsidence of basin-filling mare basalt is aided by a thin lithosphere and inhibited by a thick lithosphere (Melosh, 1978; Solomon and Head, 1980). Solomon and Head (1980) suggested that a lithospheric thickness of about 75 km has prevented graben formation in the Crisium, Nectaris, and Smythii basins. The crust in the region of the seismic stations on the southwest nearside is 45 to 60 km thick (chap. 1). Because arcuate grabens have formed in this seismically explored region, such crustal thicknesses apparently facilitate mare subsidence and graben formation. Because the estimates of lithospheric and crustal thickness are similar in magnitude, the feldspathic crust and the elastic lithosphere were probably equivalent at the time of graben formation. The mantle constituted the more plastic asthenosphere.

Chapter 4 suggests that the Procellarum-basin impact exerted a major control over crustal (lithospheric) thickness (fig. 6.22). Consequently, arcuate grabens are restricted almost entirely to the interior of that basin (pl. 5). Even the old shallow basin Tranquillitatis and the thin basalt of Mare Tranquillitatis, which lie inside Procellarum, are cut by marginal grabens (fig. 6.11). Lithospheric thickness related to Procellarum also may be reflected in the gravity structure. Outside Procellarum, even such relatively thin maria as Nectaris, Orientale, and Smythii preserve mascons. Despite their thinness, these maria lie at low elevations (more than 3.5 km below the average lunar sphere, 1,738 km in radius; fig. 6.23; table 6.1).

Thus, the thick lithosphere apparently hindered isostatic uplift of basins, extrusion of mare basalt, sinking of mascons, and formation of grabens. Each condition was opposite inside Procellarum. Oceanus Procellarum and Mare Tranquillitatis, though areally large, have only small, local gravity highs (one part of southern Procellarum and the mare-ridge feature Lamont in Tranquillitatis; figs. 11.1, 11.9; Scott, 1974). The superisostatic loads per unit area in Imbrium and Serenitatis are smaller than would be expected from their thick mare-basalt sections (table 6.1; Solomon and Head, 1980). Apparently, the thin lithosphere inside Procellarum abetted early isostatic uplift of such basins as Tranquillitatis and permitted later isostatic sinking in response to loading even by thin basalt. The concentration of maria in Procellarum and in the superposed basins is another result of the thinner lithosphere. Although mascons are not known on the farside, the depth of the giant South Pole-Aitken basin (5–7 km; Stuart-Alexander, 1978), the paucity of farside maria except in the basins superposed on South Pole-Aitken (pl. 4), and the absence of grabens all suggest farside lithospheric thicknesses at least as great as those on the non-Procellarum nearside.

The factors that localize the straight rilles are less clear but may be further effects of the Procellarum basin. The complex system along the west Procellarum shore comprises the grabens most likely to be related to this giant basin. Widespread extension of the Procellarum margin is suggested by the trends and extent of the fracture system, which are consistent with a broad regional uplift of the mantle under the basin.

More speculatively, the many straight rilles on the central and east-central nearside may have a similar origin. Mantle uplift beneath the Procellarum basin may explain the 1,600-km-long system and such "Imbrium-radial" faults as Rupes Recta, the grabens cutting the Fra Mauro peninsula (fig. 5.8), and the Cauchy set. Continuation of mild uplift into the time of mare-basalt extrusion would account for the otherwise-puzzling transection of the maria by these faults. The Triesnecker system, whose overall orientation diverges from others in its vicinity, may have been localized by Sinus Medii, whose southeast boundary is a Procellarum ring (pl. 4; fig. 5.26). Sinus Medii may have been isostatically uplifted because of viscous relaxation of the weak lithosphere, in the manner of a fractured crater floor. Tides, relaxation of a tidal bulge (Melosh, 1977), or some other global effect would seem to be attractive alternative causes of the deformation of this near-Earth zone. To my knowledge, however, the observed distribution of lunar faults is inconsistent with any of the global mechanisms that have been thus far proposed. The Triesnecker system and the systems of long straight grabens, therefore, provide additional examples of basin-related alternatives to global origins for lunar structures.

A progressive thickening over time of the lunar lithosphere in all regions (Howard, 1970) is evidenced by increasing resistance to deformation (Solomon and Head, 1980). The arcuate and straight grabens cut terra units and old mare units (chap. 11), whereas the ridges deform both old and young mare units (Lucchitta and Watkins, 1978). Thus, the graben opening was the first deformation to cease. Mare extrusion ceased somewhat later, when the elastic lithosphere exceeded 100 km in thickness (Solomon and Head, 1979). Presumably, most previous conduits for ascent of mare magmas were shut off. Wrinkling of the central mare surfaces and crater-floor uplift were the longest enduring modifications. All these changes were presumably the result of general global cooling. Decreasing plasticity of part of the mantle added thickness to the lithosphere, which once consisted only of the terra crust. Although the mascons indicate that the superisostatic loads still exist, continued subsidence is unlikely because endogenic moonquakes do not all correlate with maria (Nakamura and others, 1979; Solomon and Head, 1979). If any asthenosphere remains today, it is too deep to affect surface deformation. The only recent deformation that has been suggested since analysis of the Apollo results is minor thrust faulting in the terrae (Binder, 1982).

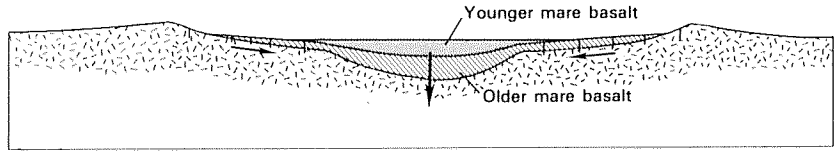


FIGURE 6.12.—Diagrammatic cross section showing stresses responsible for graben opening and ridge formation during subsidence of mare basalt in a double-ringed basin. Short vertical lines cutting older mare unit and underlying basin material denote grabens.

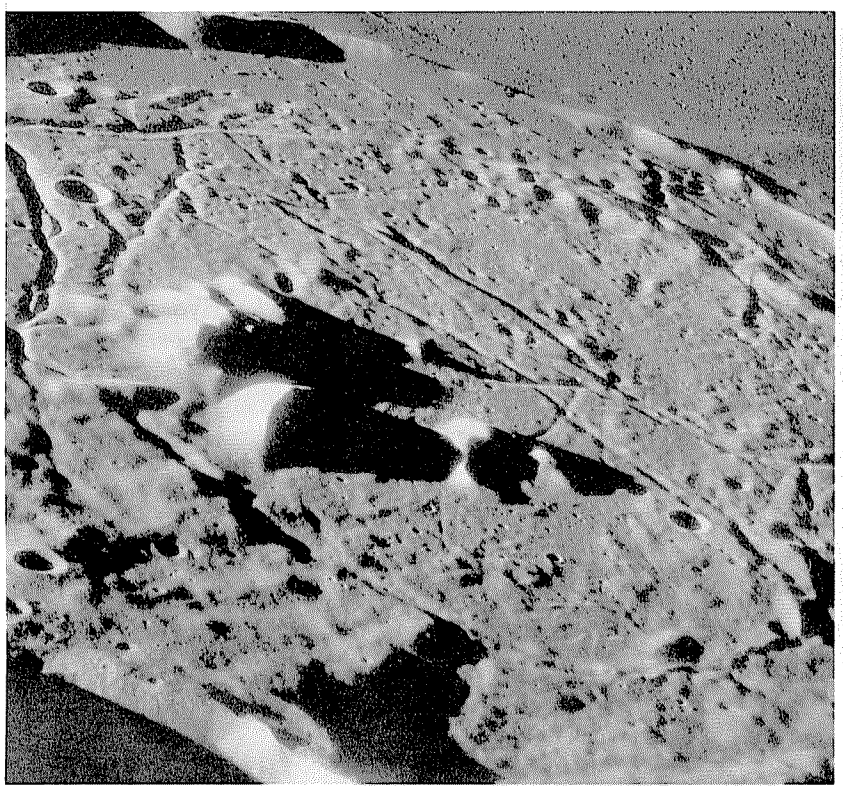

A

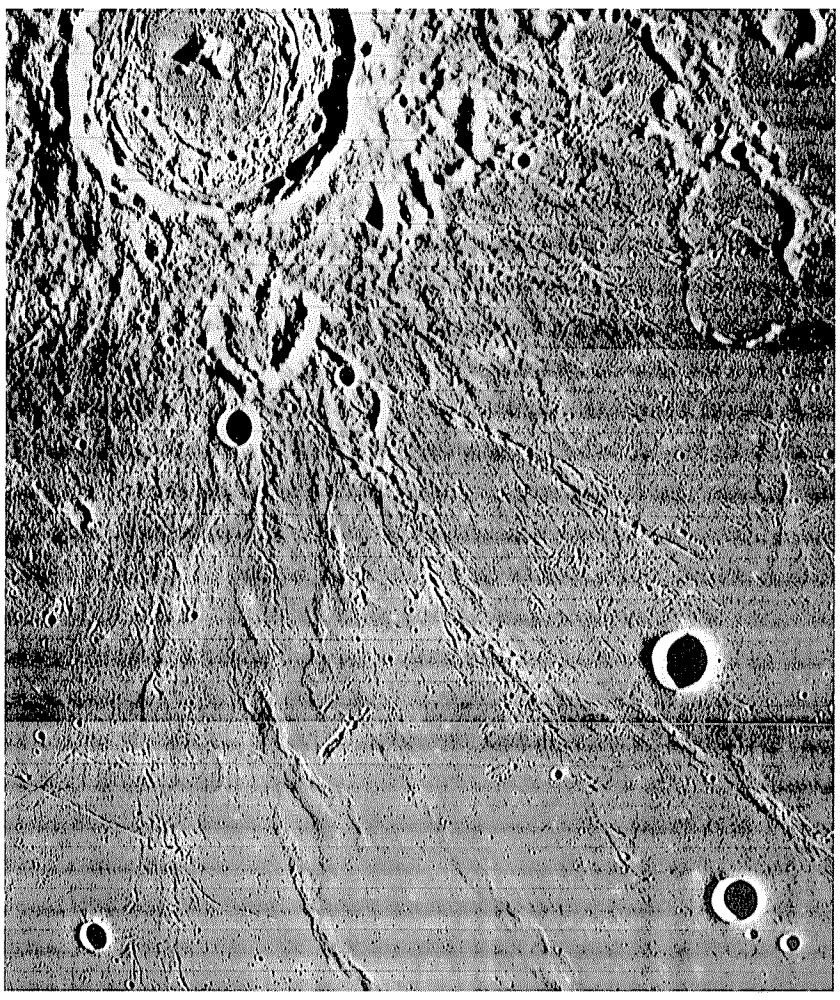

B

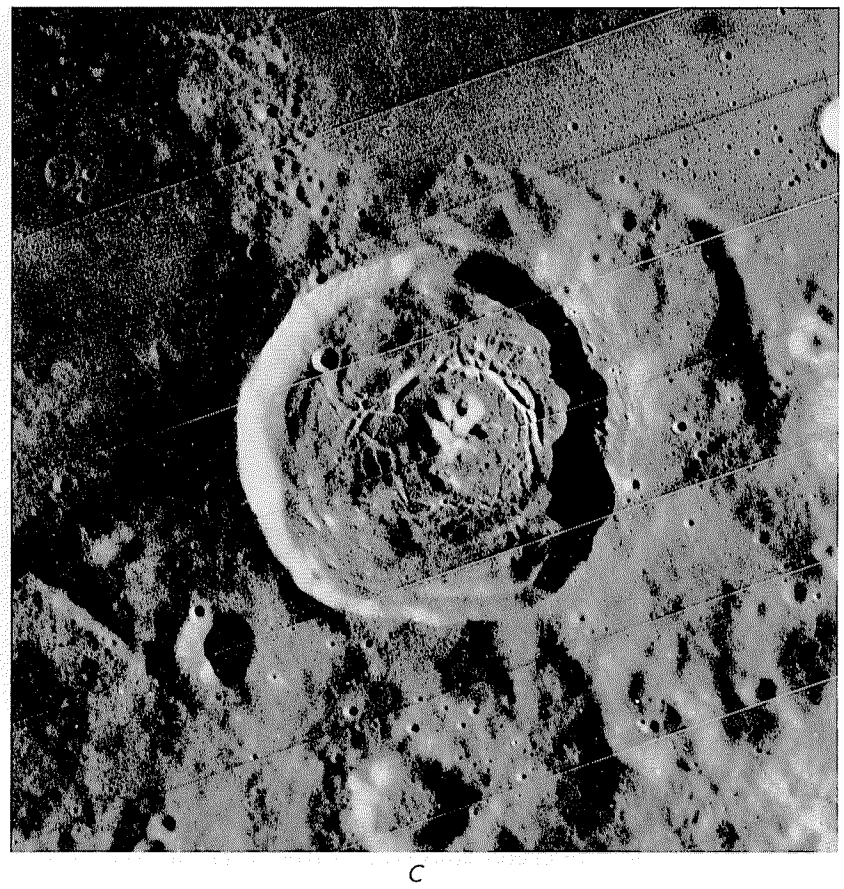

C

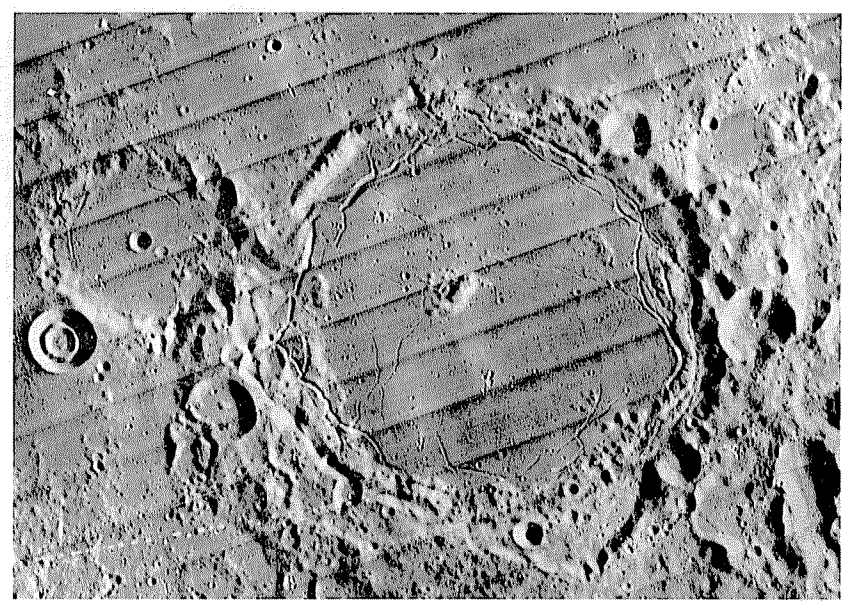

D

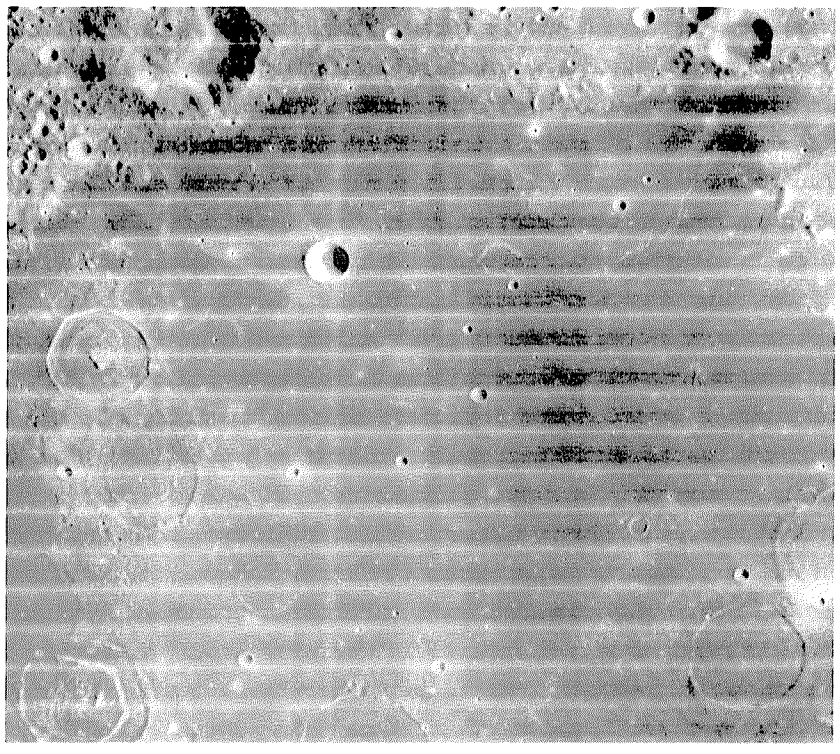

E

FIGURE 6.13.—Raised fractured floors of craters.

*A.* Gassendi (110 km, 17.5° S., 40° W.), on north border of Mare Humorum. Floor is almost as high as mare, but peaks indicate impact origin. View southward. Apollo 16 frame H–19295.

*B.* Taruntius (56 km, 5.5° N., 46.5° E.), on northwest border of Mare Fecunditatis, a typical fresh impact crater except for raised floor. Orbiter 1 frame M–31.

*C.* Vitello (42 km, 30.5° S., 37.5° W.), on south margin of Mare Humorum, with dark-mantled rim and very fresh fractures on uplifted floor. Orbiter 4 frame H–136.

*D.* Pitatus (97 km, 30° S., 13.5° W.), on south border of Mare Nubium. Concentric rilles result from uplift of crater floor and later mare fill. Small bull's-eye crater at left may have similar cause. Chain of craters at right are secondary-impact craters of Imbrium basin. Line of white dots in lower left is photoprocessing artifact. Orbiter 4 frame H–119.

*E.* Group of double-ringed craters, 30 to 35 km in diameter, in Mare Smythii. Cylinderlike uplift of floor is indicated (fig. 6.15). Orbiter 4 frame H–17.

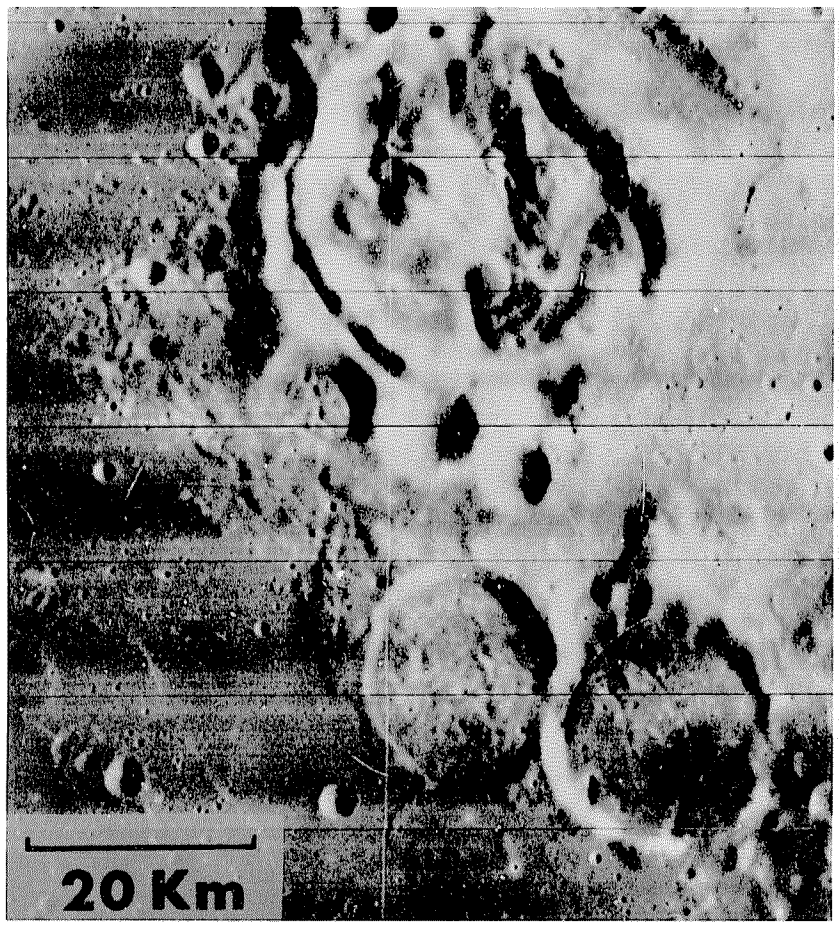


*F*

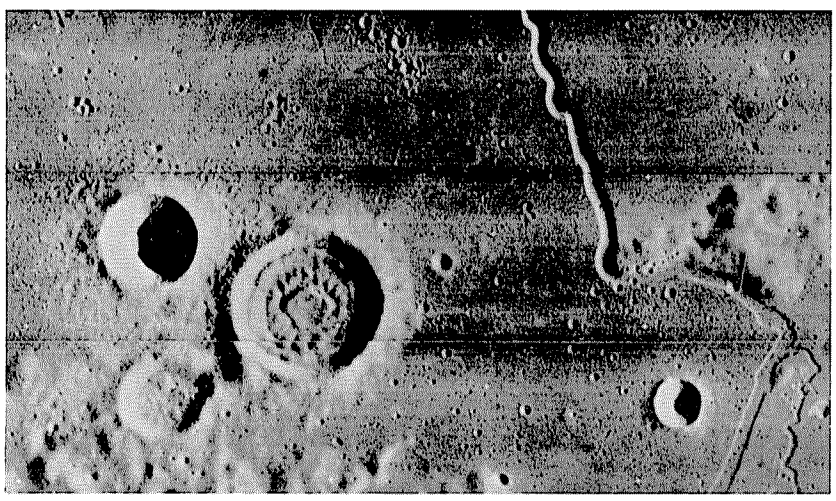

*G*

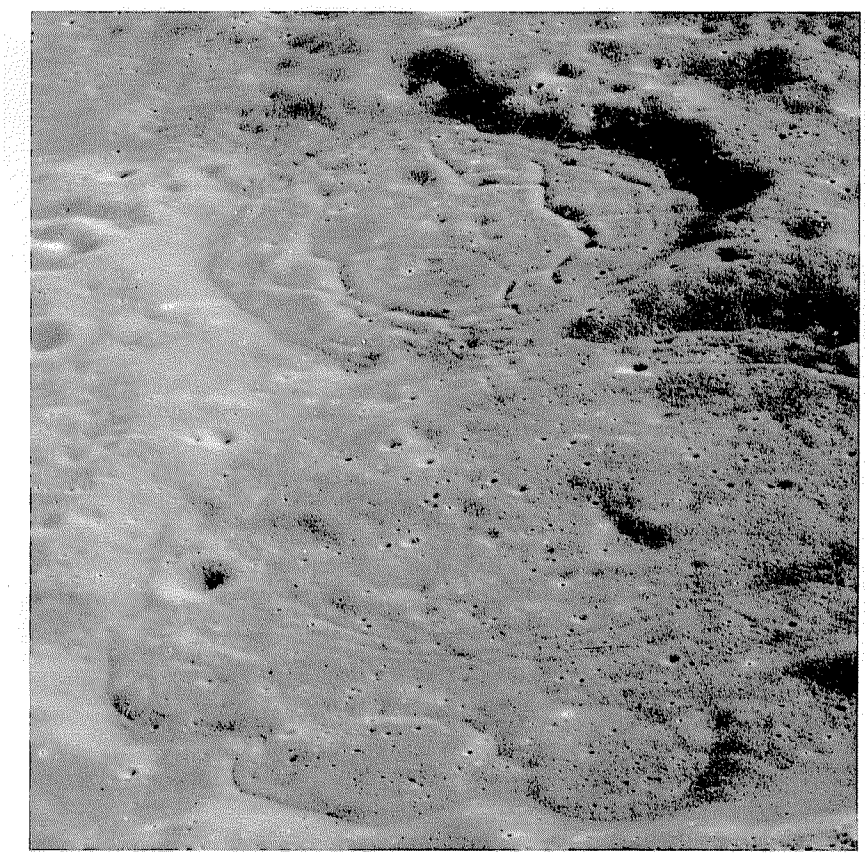

*H*

*F.* Gaudibert (34 km, 11° S., 38° E.) and two smaller craters on margin of Mare Nectaris. Bulbous landforms are possible evidence for viscous extrusive volcanism (Elston, 1972) but were probably created by extensive uplift (Brennan, 1975). Dark-mantling material surrounds teardrop crater along fracture in lower right crater. Orbiter 4 frame H–72.

*G.* Liouville DA (11 km, 46.5°, 52° W.), on border of Sinus Roris, possibly containing volcanic extrusions (Scott and Eggleton, 1973) but probably another uplift phenomenon. Sinuous rille Rima Sharp I is at right. Orbiter 4 frame H–163.

*H.* Tamm (38 km, 4.5° S., 146.5° E., foreground) and Van den Bos (32 km), 225 km southeast of Mendeleev-basin rim, filled by fissured, viscous-appearing material possibly emplaced as impact melt of Mendeleev. View southward. Apollo 10 frame H–4966.

TABLE 6.1.—*Physical properties of major nearside basins containing large maria*

[D, diameter (km); basin D's from table 4.1.
Average elevation: Elevation of central mare inside obvious sloping margins, in km below 1,738-km datum (S.S.C. Wu, written commun., 1983).
Mascon mass: excess mass in units of $10^{20}$ g (compiled by Solomon and Head, 1980, table 2).
Mascon load: superisostatic load in center of mare, in units of $10^{8}$ dyne/cm$^2$ (calculated by Solomon and Head, 1980, table 2, using different mare diameters than those listed here; they took Smythii as 340 km, Grimaldi as 100 km, and Nectaris as 400 km in diameter)]

| Basin | Basin D | Mare D | Ratio | Outer D of graben zone | Ratio to basin | D of 1-km isopach | Ratio to basin | Ratio to mare | Average elevation | Mascon mass | Mascon load |
|---|---|---|---|---|---|---|---|---|---|---|---|
| Imbrium (with Frigoris). | 1,500 | 1,450 | --- | --- | --- | --- | --- | --- | --- | --- | --- |
| Imbrium (without Frigoris). | 1,160 | 960 | .83 | 1,160 | 1.00 | 350 | .30 | .35 | 2.5-3.5 | 23.0 | .9 |
| Crisium---------- | 1,060 | 420 | .40 | <420 | <.40 | 210 | .20 | .50 | 4.0-4.5 | 9.4 | 1.3 |
| Orientale--------- | 930 | 280 | .30 | 500 | .54 | 150(?) | .16(?) | .54 | 4.0 | 3.3 | .9 |
| Nectaris---------- | 860 | 300 | .35 | 320 | .37 | 150 | .17 | .50 | >3.5 | 9.0 | 1.3 |
| Smythii----------- | 840 | 200 | .24 | <200 | <.24 | 0 | 0 | 0 | 4.0-4.5 | 5.0 | 1.4 |
| Humorum----------- | 820 | 350 | .43 | 750 | .91 | 125 | .15 | .36 | ? | 5.2 | 1.4 |
| Tranquillitatis--- | 775 | 600 | .77 | 710 | .92 | 150 | .19 | .25 | 1.5->2.5 | 0 | 0 |
| Serenitatis------- | 740 | 600 | .81 | 850 | 1.15 | 300(?) | .41 | .50 | 3.0-4.0 | 14.0 | 1.3 |
| Fecunditatis------ | 690 | 600 | .87 | 600 | .87 | 150 | .22 | .25 | 2.0-3.0 | 0(?) | 0(?) |
| Nubium------------ | 690 | 600 | .87 | 620 | .90 | 0(?) | 0(?) | 0(?) | >3.0 | 0 | 0 |
| Humboldtianum----- | 600 (each) | 120 | .20 | <120 | <.20 | 0(?) | 0(?) | 0(?) | ? | 0(?) | 0(?) |
| Grimaldi---------- | 430 | 150 | .35 | 360 | .84 | 0(?) | 0(?) | 0(?) | 3.0-3.5 | .76 | 1.4 |

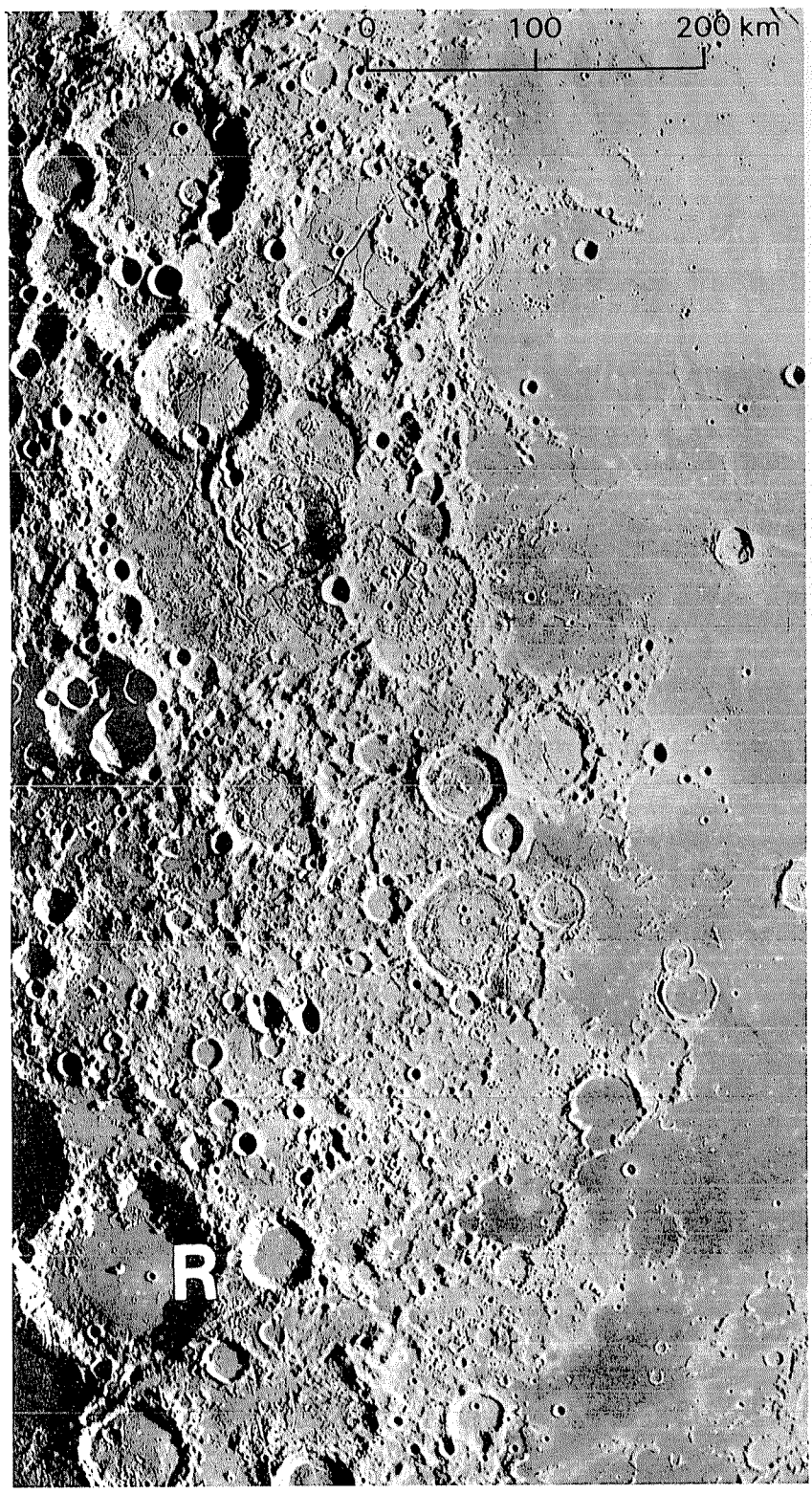


FIGURE 6.14.—Numerous fractured-floor craters along west border of Oceanus Procellarum between lat 28° N. and 57° N. R, crater Röntgen (126 km, 33° N., 91° W.), superposed on Lorentz basin. Linear structure at bottom is radial to Imbrium basin. Orbiter 4 frame H–183.

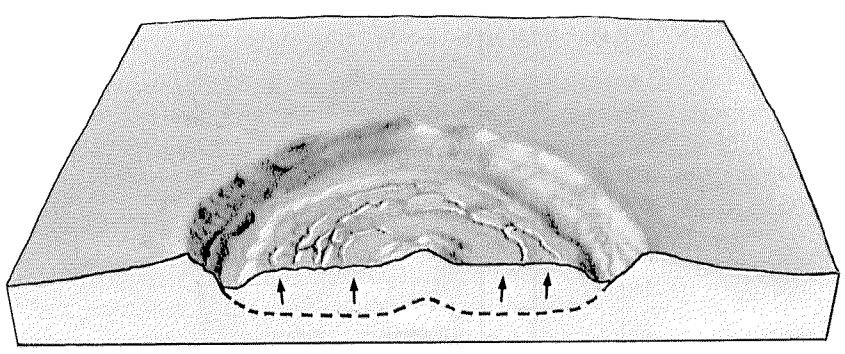

FIGURE 6.15.—Crater floor uplifted (arrows) from original position (dashes) lower than surrounding terrain.

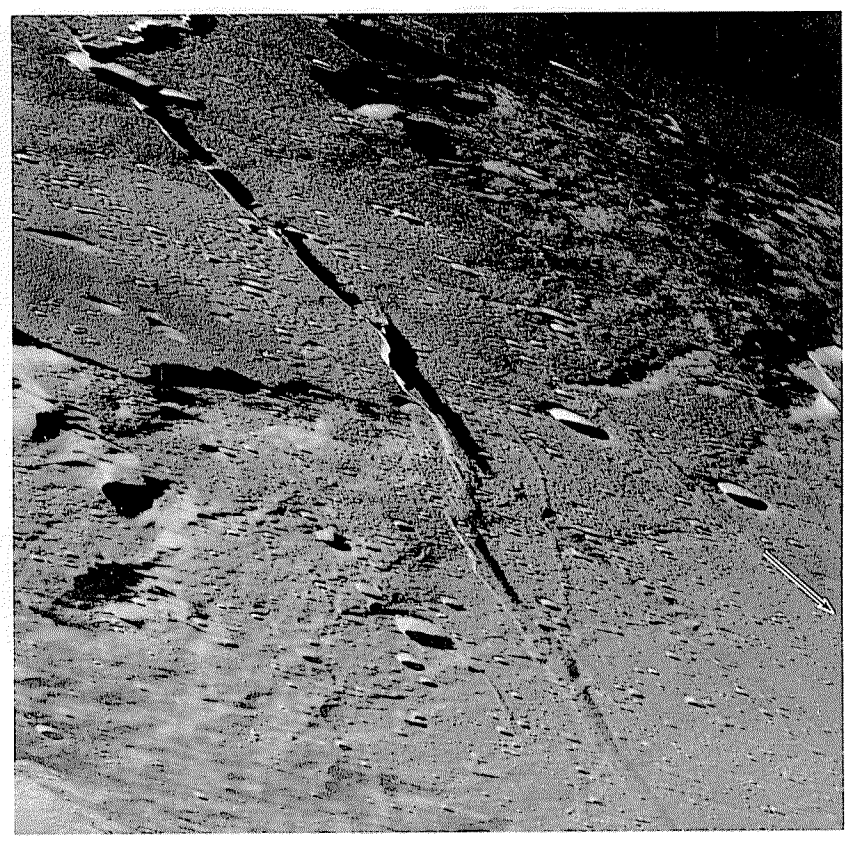

*A*

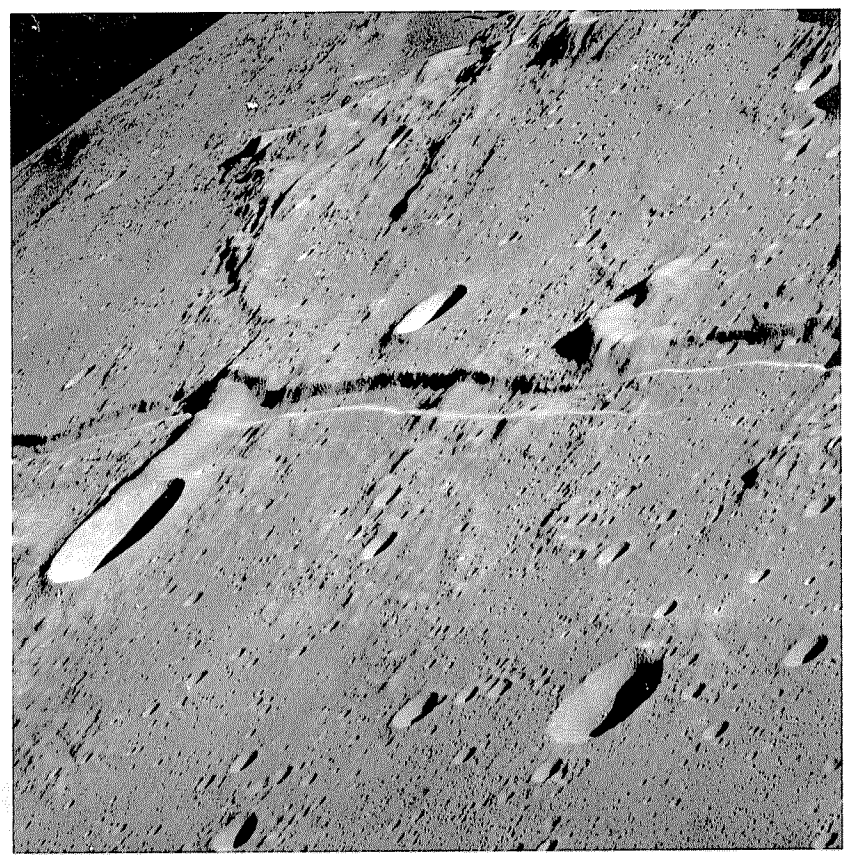

*B*

FIGURE 6.16.—Straight rilles Hyginus (*A*) and Ariadaeus (*B*). Rima Ariadaeus continues westward in *B* as rille indicated by arrow in *A*. Largest crater in *B* is Silberschlag (13 km, 6° N., 6.5° E.). Surface offsets and echelon patterns are obvious. Apollo 10 frames H-4648 (*A*) and H–4645 (*B*).

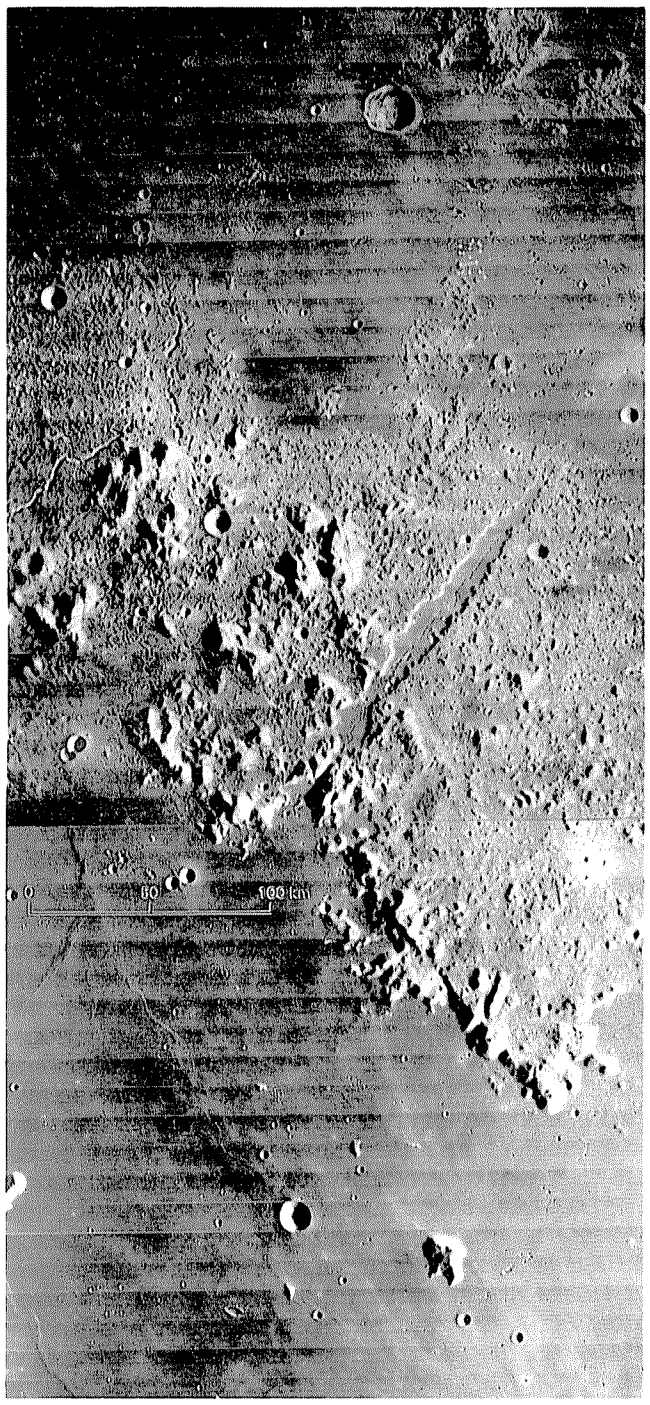


A

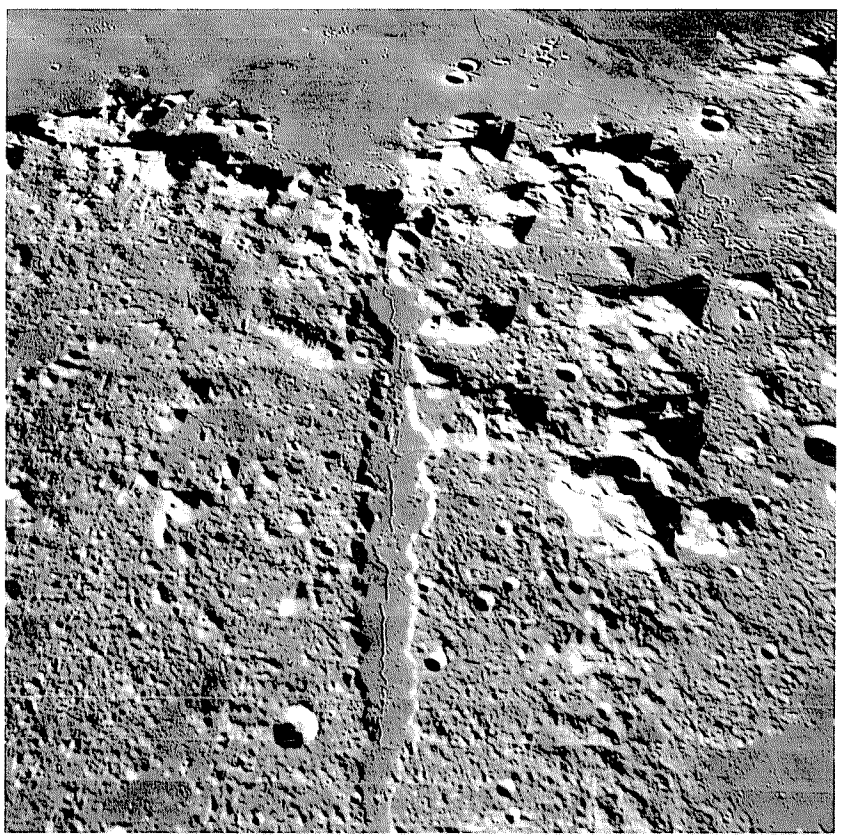

B

FIGURE 6.17.—Vallis Alpes (Alpine Valley), 200 km long and oriented radially to Imbrium basin. Knobby material is Alpes Formation (see chaps. 4, 10).
*A*. Regional setting, centered 47° N., 0°. Orbiter 4 frame H–115.
*B*. Detail. View southwestward. Orbiter 5 frame H–102.

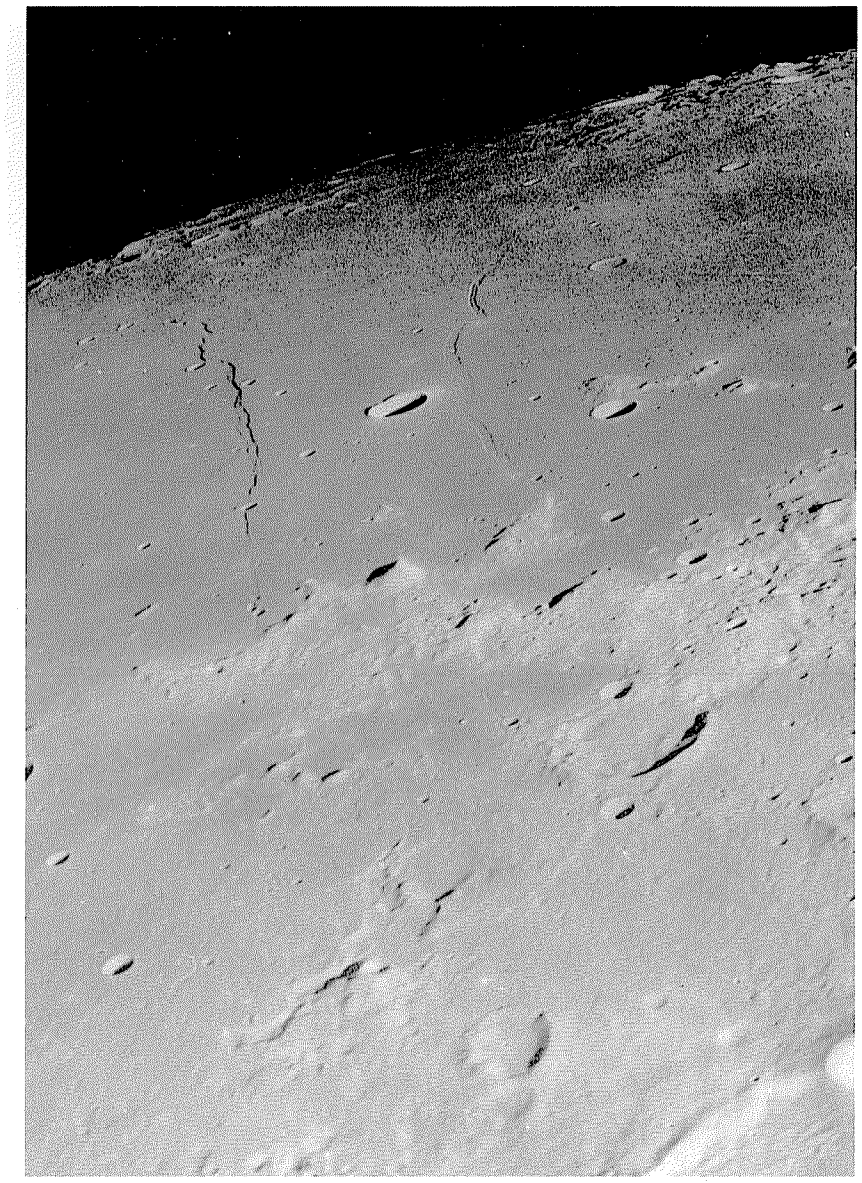

FIGURE 6.18.—Mare Tranquillitatis, faulted by Cauchy rille (Rima Cauchy, right) and complex scarp (Rupes Cauchy, left), oriented radially to Imbrium basin (beyond top of photograph). Fresh crater between the two structures is Cauchy (12 km, 10° N., 39° E.). Part of crater Taruntius (compare fig. 6.13*B*) is visible in lower right corner. Apollo 11 frame H–6231.

FIGURE 6.19.—Grabens cutting Mare Fecunditatis, crater Goclenius (longest dimension, 72 km; 10° S., 45° E.), and mare fill of Goclenius. View southwestward. Apollo 8 frame H–2225.

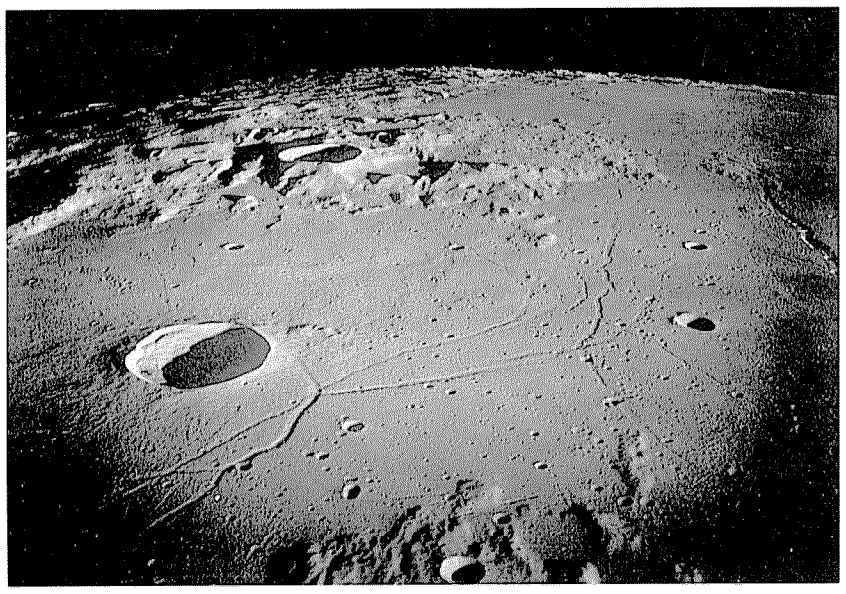

FIGURE 6.20.—Triesnecker system of grabens east of crater Triesnecker (left center; 26 km, 4° N., 3.5° E.). Part of northwest branch of Rima Hyginus is at right, oriented northwest radially to Imbrium basin. Apollo 10 frame H–4816.

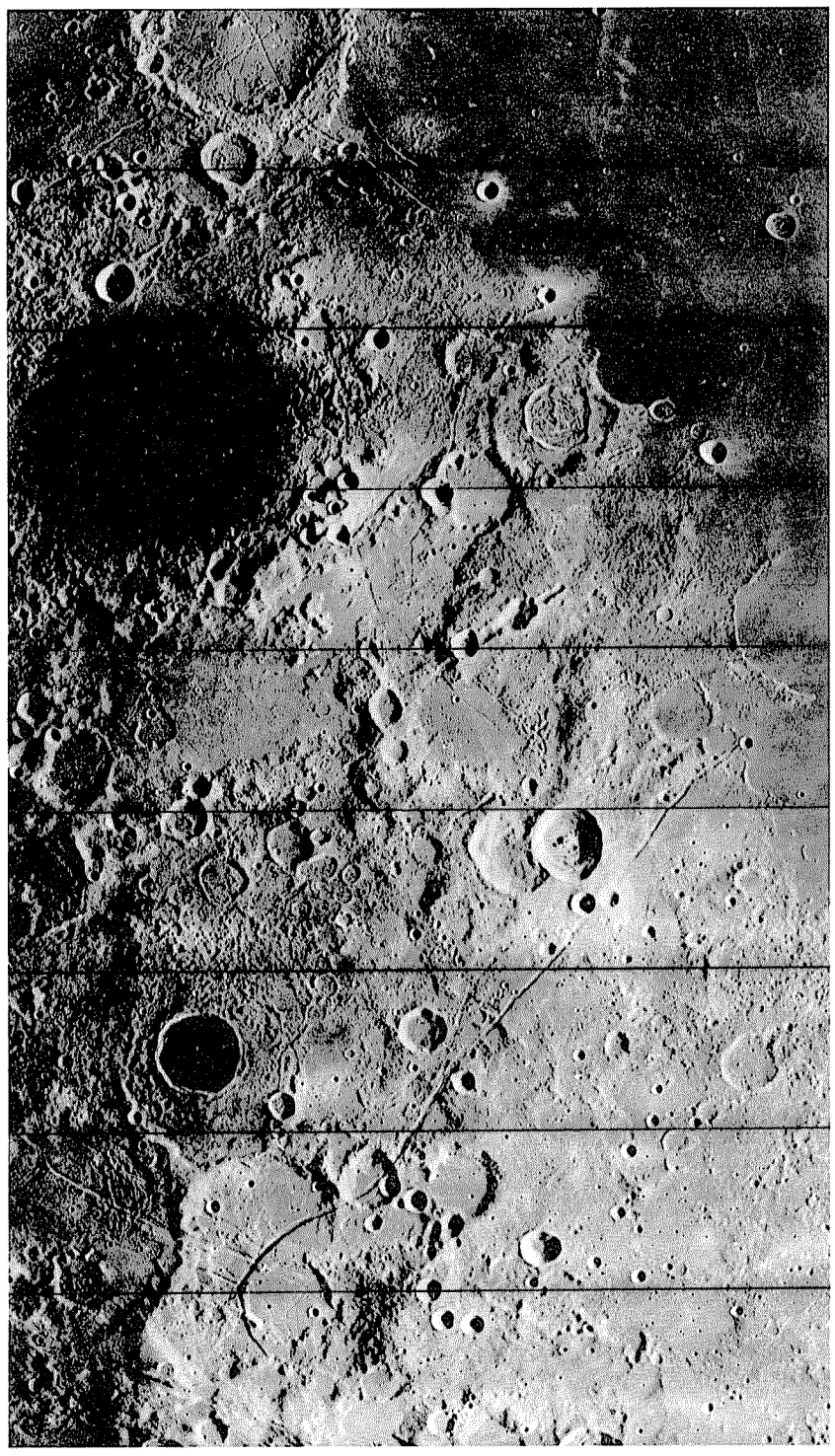

FIGURE 6.21.—Grabens along west margin of Oceanus Procellarum south of crater Hevelius (106 km, 2° N., 67° W., cut by top edge of photograph). Circular mare below Hevelius fills Grimaldi basin (compare fig. 4.4*H*). Orbiter 4 frame M–161.

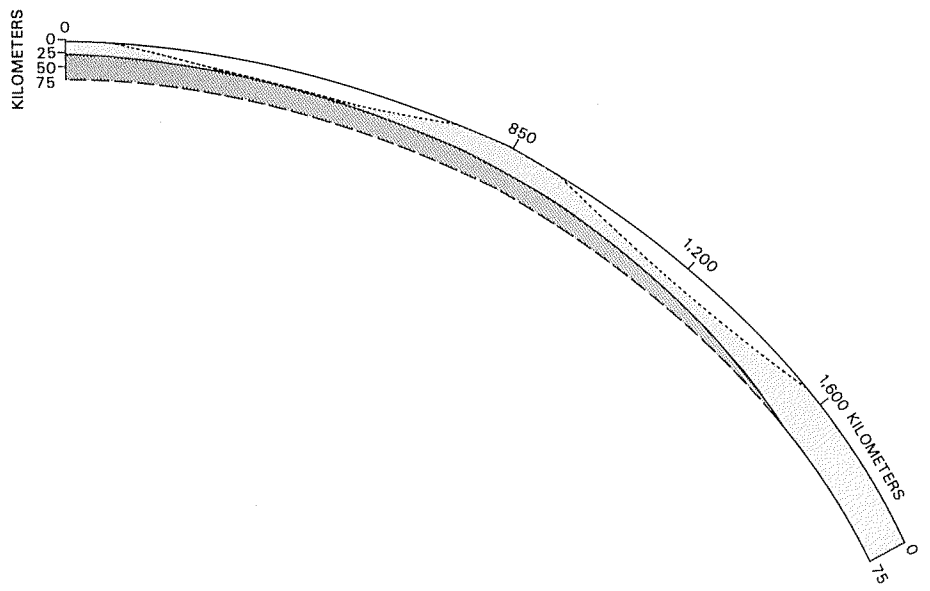


FIGURE 6.22.—Diagrammatic cross section of half of Procellarum basin, showing interpreted crustal thinning from 75 km outside basin to 25 km in basin center, caused by excavation and mantle uplift; dashed line denotes preimpact position of mantle-crust interface (lunar Moho). Ring radii (Whitaker, 1981) are shown above lunar surface; basin rim is at 1,600 km. Dotted lines denote additional excavation and crustal thinning by later basins; basin in Procellarum center penetrates crust to mantle, but same-size basin in intermediate and outer Procellarum troughs bottoms in crust. Vertical and horizontal dimensions and curvature to true scale. Surface relief and relative relief of concentric rings and shelves are barely detectable.

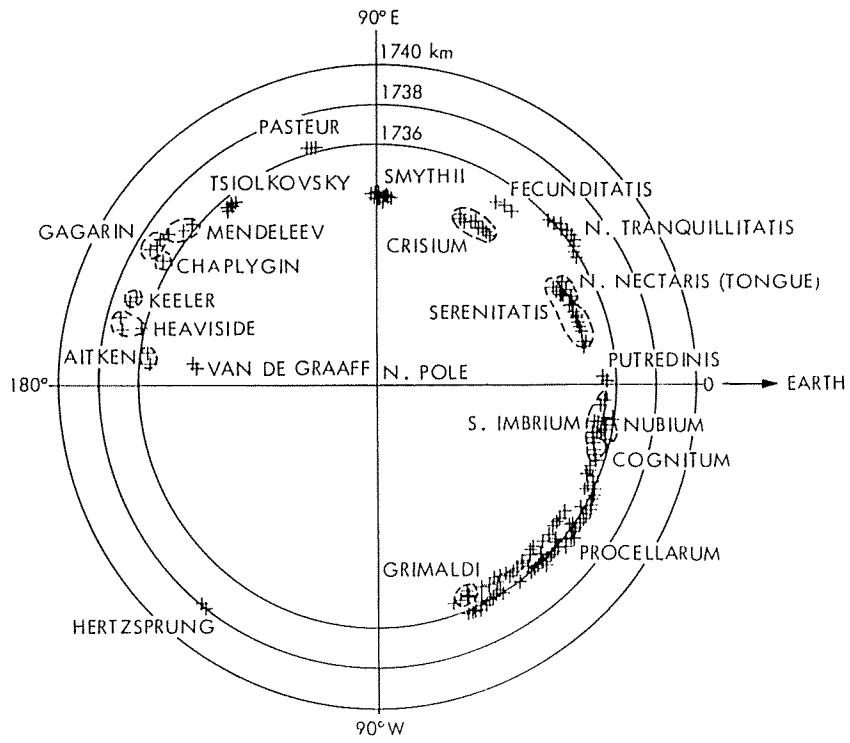


FIGURE 6.23.—Elevations of lunar maria compared with those of the terrae, most of which define a sphere 1,738 km in radius about the center of gravity (Sjogren and Wollenhaupt, 1976). Derived from laser altimetry and photogrammetry obtained during Apollo 15 and 16 missions (Kaula and others, 1973, 1974; Sjogren and Wollenhaupt, 1976). Smythii, Crisium, Serenitatis, Imbrium (S. Imbrium), and Grimaldi vary in elevation, although all have large mascons. Elevations of maria in Aitken, Tsiolkovskiy, and Van de Graaff probably reflect elevations of crater floors; Aitken is on rim of South Pole-Aitken basin, and van de Graaff well inside. Chaplygin, Gagarin, Heaviside, Hertzsprung, Keeler, Mendeleev, and Pasteur are filled by terra plains, not maria. Polar plot relative to 1,738-km-radius sphere about lunar center of gravity.